Sedimentary Geology 449 (2023) 106371

Contents lists available at ScienceDirect

Sedimentary Geology

journal homepage: www.elsevier.com/locate/sedgeo

Evolution of the Exmouth-Barrow carbonate margin through the Miocene: Insights from 3D seismic data and field investigations (North West Shelf, Australia)

Rosine Riera [a,b,*], Victorien Paumard [b,c], Julien Bourget [b], Tony Allan [d], Ulysse Lebrec [a,b]

[a] Norwegian Geotechnical Institute, Level 7, 40 St Georges Terrace, Perth, WA 6000, Australia
[b] Centre for Energy and Climate Geoscience, School of Earth Sciences, The University of Western Australia, 35 Stirling Highway, Perth, WA 6009, Australia
[c] UWA Oceans Institute, The University of Western Australia, Perth, WA 6009, Australia
[d] School of Geosciences, The University of Sydney, NSW 2006, Australia

ARTICLE INFO

Article history:
Received 8 January 2023
Received in revised form 15 March 2023
Accepted 16 March 2023
Available online 23 March 2023

Editor: Dr. Brian Jones

Keywords:
Miocene
Seismic stratigraphy
Seismic geomorphology
Carbonate margin
Climate Optimum
Ramp to rimmed shelf

ABSTRACT

Carbonate margins are records of the palaeoclimatology, palaeoceanography and palaeogeography of continental shelves, and their study can help identify both regional and global palaeoenvironmental changes. This study documents the evolution of the Exmouth-Barrow margin, which records one of the largest ramp to rimmed platform transition documented yet, throughout the Miocene. The research is based on the integration of onshore outcrops, offshore wells and 3D seismic data.

The margin evolution can be divided in four main phases, including: (1) progradation of carbonate clinoforms, forming a depositional ramp, during the early Miocene; (2) sabkha development and extensive dolomitization, concomitant with the Miocene Climatic Optimum; (3) formation of a carbonate barrier-lagoon system associated with slope channels during the middle Miocene; and (4) onset of a dominantly siliciclastic sedimentation from the end of middle Miocene onward.

Overall, this study illustrates how outcrops and offshore seismic data can be integrated to reconstruct the regional stratigraphic and palaeoenvironmental evolution of a continental margin, with outcrops providing precise but local information, while 3D seismic data allow the basin-scale reconstruction of the palaeolandscape.

1. Introduction

The Miocene period (~23–5 Ma) is a time of major climatic changes. While being part of the Cenozoic overall transition from a warm world with ice-free poles to a cooler world with permanent ice-sheets, the early part of the Miocene records a global warming which reaches its acme during the Miocene Climatic Optimum (MCO; Flower and Kennett, 1994; Holbourn et al., 2015; Zachos et al., 2001, 2008). The MCO was up to 7 °C warmer than today (Steinthorsdottir et al., 2021), and is recorded between ~17 Ma and 14.8 Ma (Sangiorgi et al., 2018). It is followed by a transition period to cooler conditions, the Middle Miocene Climatic Transition (MMCT), that happened from ~15 Ma to ~14/13 Ma (respectively for high and low latitudes; Mudelsee et al., 2014).

Parallel to these global events, there is an acme of reef development during the early to middle Miocene (Burdigalian-Serravallian; Perrin, 2002), including the development of reefs all along the Australian North West Shelf (NWS) during the middle Miocene (Anell and Wallace, 2020; McCaffrey et al., 2020; Ryan et al., 2009). The global cooling subsequent to the MMCT is marked by an expansion of the Antarctic ice sheets, high-amplitude sea level variations, invigoration of ocean currents, increased continental aridity in mid-latitude regions, including Australia, and marine biota turnover (Flower and Kennett, 1994; Frigola et al., 2021, 2018; Holbourn et al., 2005; Shevenell et al., 2004). The development of the East Antarctic Ice Sheet at the end of the middle Miocene (13.6–11.4 Ma) is linked to a sea level fall of 50.0 ± 5.0 m (John et al., 2004), and the development of carbonate platforms whose morphology is shaped by currents (Betzler and Eberli, 2019). Global cooling and ice sheet expansion continued throughout the late middle Miocene and late Miocene (Flower and Kennett, 1994; Frigola et al., 2018; Herbert et al., 2016; Holbourn et al., 2018; Zachos et al., 2008), which gradually led to modern oceanographic and climatic conditions.

Detailed studies of palaeoenvironmental conditions are traditionally conducted on basin deposits, which have the potential to record continuous sedimentary successions over long periods of time (e.g., Holbourn et al., 2018; Leutert et al., 2020; Liebrand et al., 2016). Carbonate

* Corresponding author at: Norwegian Geotechnical Institute, Level 7, 40 St Georges Terrace, Perth, WA 6000, Australia.
E-mail address: rosine.riera@ngi.no (R. Riera).

https://doi.org/10.1016/j.sedgeo.2023.106371

margins, which are created by an accumulation of bioclasts (i.e., skeletons) and chemically precipitated particles, also have the potential to record such palaeoenvironmental and palaeoceanographic changes through facies analysis (Mutti et al., 2010) and seismic geomorphology (Davies et al., 2004; Posamentier et al., 2007).

The Miocene strata of the North West Shelf of Australia (NWS) are observable through extensive offshore 3D seismic data (Paumard et al., 2019b), outcrops and offshore wells (Fig. 1). As such, the NWS is an ideal location to study the evolution of a Miocene carbonate margin using outcrops, wells and 3D seismic data, and to correlate the inferred regional palaeoenvironmental changes observed to global Miocene climatic events. In this context, this study focuses on the Miocene evolution of the carbonate margin located in the Exmouth-Barrow sub-basins (Northern Carnarvon Basin, southernmost part of the NWS), as the stratigraphy can be followed from onshore outcrops to offshore 3D seismic datasets, hence providing a unique opportunity to perform a multi-scale analysis of the evolution of a carbonate-dominated margins during the Miocene. The study aims at reconstructing the stratigraphic and geomorphologic evolution of this margin through the Miocene, and at documenting: (1) the successive palaeodepositional environments observed in the subsurface offshore, using seismic geomorphology; and (2) the different lithologies observed from outcrops and offshore wells. The Miocene palaeoenvironmental evolution of the area through time is then presented.

2. Geological setting

The North West Shelf (Purcell and Purcell, 1988) is a ~2400 km long passive continental margin located along the north-western border of Australia, between ~11°S and ~22°S. Since the Cambrian, it was formed through multiple rifting and aborted rifting events related to the fragmentation of Gondwanaland and then Pangea (Keep et al., 2007; Purcell and Purcell, 1988; Yeates et al., 1987). During this fragmentation, margin-parallel basins were formed along the NWS (Longley et al., 2002), including, from south to north, the Northern Carnarvon Basin, the Roebuck Basin, the Browse Basin and the Bonaparte Basin (I'Anson et al., 2019). Phases of aborted intra-cratonic rifting created elongated sub-basins, including the Exmouth and Barrow sub-basins in the southern part of the NWS (Fig. 1). These basins and sub-basins were major depocenters during different periods of the Mesozoic, and they hold important oil and gas reserves (I'Anson et al., 2019). The Exmouth, Barrow and the other Mesozoic sub-basins of the NWS were filled by thick sedimentary successions by the end of the Mesozoic, and Cenozoic sedimentation along the NWS is then independent from rift-basin locations (Apthorpe, 1988). However, the location of Mesozoic sub-basins is commonly used as scheme for naming geographic areas in studies focusing on Cenozoic strata of the NWS (Apthorpe, 1988; Elders and Bernecker, 2019), and this convention is followed in this study. During the Neogene, a regional subsidence episode driven

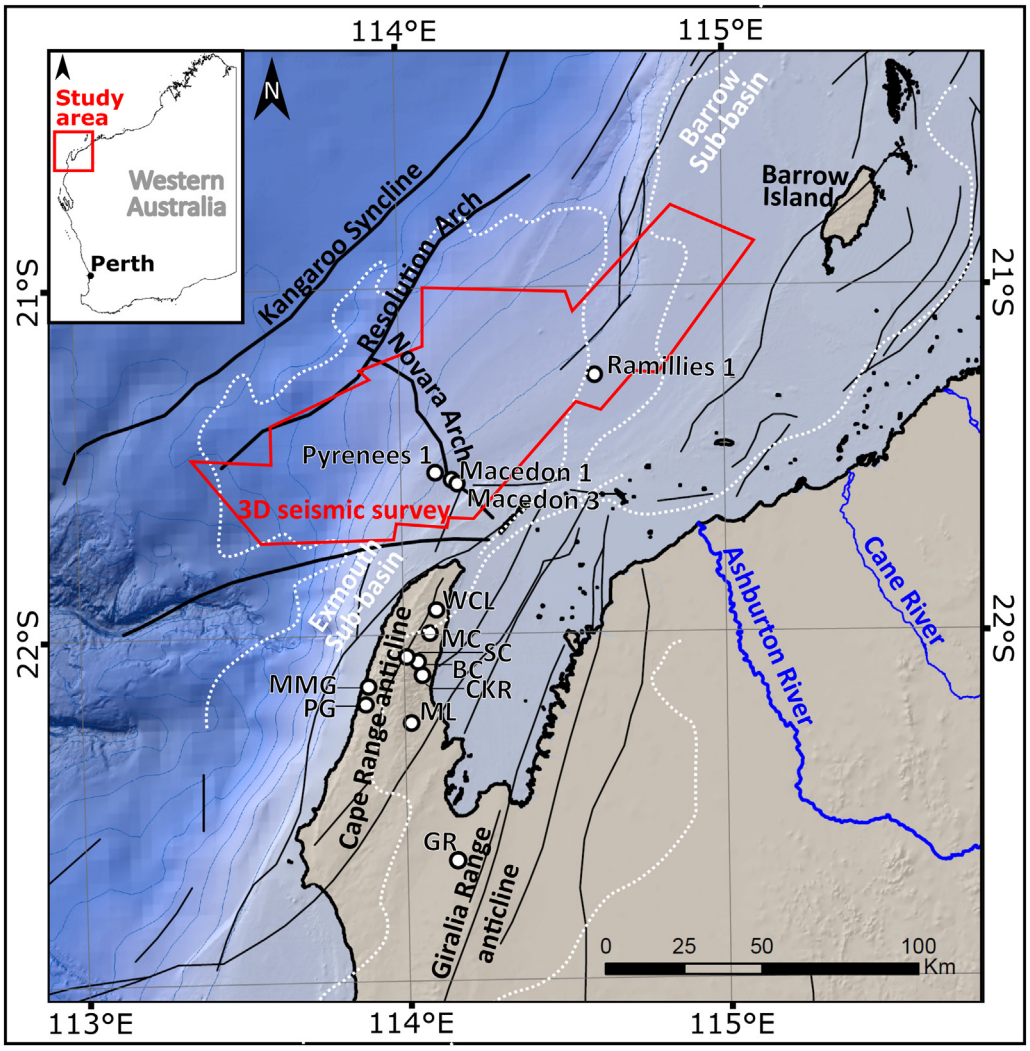

Fig. 1. Location map of the study area highlighting the location of the seismic survey analysed (in red, data courtesy of PGS), and of wells and outcrops investigated (white dots). Structures are after I'Anson et al. (2019) and Tindale et al. (1998). Rivers are after Crossman and Li (2015). MMG: Mandu Mandu Gorge, PG: Pilgonaman Gorge, WCL: Water Corporation Land, MC: Mowbowra Creek, SC: Shothole Canyon, BC: unnamed canyon north of Badjirrajirra Creek, CKR: Charles Knives Road, ML: Mount Lefroy, GR: Giralia Range.

by mantle convection has tilted the NWS (Dicaprio et al., 2011; Czarnota et al., 2013).

While the NWS has been dominantly in a passive state after the end of the Early Cretaceous rifting (Apthorpe, 1988; Marshall and Lang, 2013), localised structural inversions occurred during the Late Cretaceous (i.e., concurrent with the break-up between Australia and Antarctica; Cathro and Karner, 2006; Direen et al., 2007) and from ~25 Ma to present, with an apex during the late Miocene (concomitant with the collision between the Australian Plate and the Banda Arc; Cathro et al., 2003; Keep et al., 2007; Keep and Haig, 2010; Malcolm et al., 1991; Saqab et al., 2017). The Oligo-Miocene palaeoseafloor is dominantly shaped by these Cretaceous and Oligo-Miocene phases of compressional tectonism associated with structural inversions (Figs. 1, 2). Notable structures created by the Cretaceous structural inversions include the Novara Arch, which is NW-SE oriented and may have uplifted until the Oligocene (Driscoll and Karner, 1998; Tindale et al., 1998; Cathro and Karner, 2006). The Novara Arch divides the area investigated in two depocenters during the Oligocene and Miocene, designated here as the Southern and Northern depocenters (Fig. 2). The Resolution Arch, which is oriented perpendicularly to the Novara Arch, bounds the area investigated to the NW (Fig. 2), and was also formed by Cretaceous inversions, but with the bulk of the uplift possibly occurring during the late Miocene (Tindale et al., 1998). The Kangaroo Syncline, which is a NE-SW oriented depression located to the northwest of the Resolution Arch, was created in response to the uplift of the Resolution Arch (Tindale et al., 1998). Barrow Island, the emerged part of an anticline which started its formation during the late Jurassic (Fig. 1), was also uplifted during the Cretaceous, and then during the Cenozoic (Campbell et al., 1984; Keep et al., 2007). The Cape Range anticline and other coastal anticlines (Fig. 1) were formed by fault inversions during the Miocene or in younger times (Cathro and Karner, 2006; Hillis et al., 2008; Hocking et al., 1987; Malcolm et al., 1991; van de Graaff et al., 1976).

Strata accumulated during the post-rift phase are dominantly shales, marls and shelfal carbonates locally interbedded with sandstones (Apthorpe, 1988; Longley et al., 2002; Romine et al., 1997). Composition of these strata may have been in part controlled by the northward drift of the NWS with the Australian plate, as it migrated from sub-polar to tropical latitudes during the Cenozoic (Veevers and Cotterill, 1978; Apthorpe, 1988; Young et al., 2001). Middle Oligocene to late Miocene strata form a depositional supersequence, overlying a truncated erosional unconformity formed during a phase of major eustatic fall (Romine et al., 1997). Most of the early Oligocene strata were eroded in the Exmouth and Barrow sub-basins during this event (Romine et al., 1997).

Oligocene to early Miocene strata along the NWS are represented by prograding clinoforms whose topsets form a prograding distally steepened ramp (McCaffrey et al., 2020; Riera et al., 2022; Young et al., 2001). Their detailed morphology is known from the Dampier sub-basin area (Cathro et al., 2003) and the Browse Basin (Rankey, 2017). The shelf break was permanently submerged in water depths around 100 m (Cathro et al., 2003). While offshore seismic and well studies have traditionally presented this ramp as built by cool to subtropical heterozoan carbonates independent from the location of the photic zone (Anell and Wallace, 2020; Cathro et al., 2003; Moss et al., 2004), onshore-based studies indicate that the ramp is dominantly composed of large benthic foraminifera, with a carbonate production very much dependant on photozoan organisms (Chaproniere, 1975; Collins et al., 2006; Condon et al., 1955; Crespin, 1955). Correlation of onshore outcrops and offshore seismic data indicates that the ramp is dominantly composed of micropackstone (i.e., very fine packstone composed of undifferentiated skeletal debris, with a clayey to micritic matrix), with large benthic foraminifera present in its more proximal part (Riera et al., 2022). In the southern NWS, the proximal part of the ramp became temporarily emerged during the early to middle Miocene transition (Cathro et al., 2003; Collins et al., 2006), and sabkha

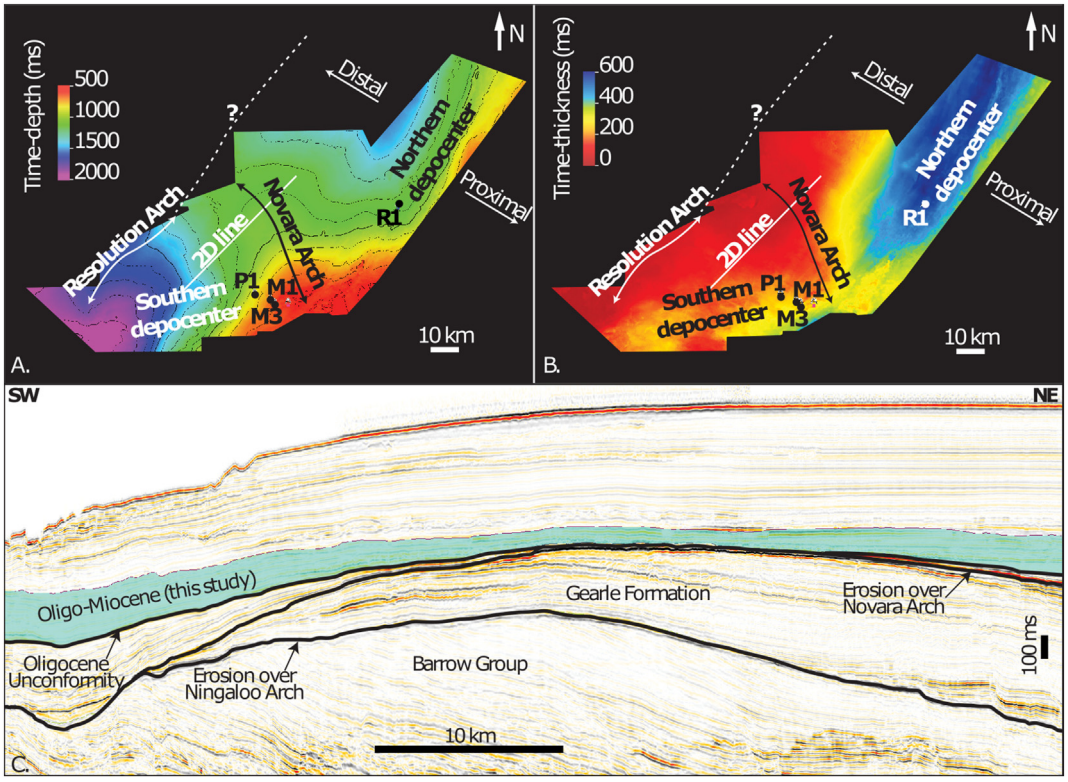

Fig. 2. A. Time-structure map (in ms TWT) of the reflector R1, located at the base of the studied interval, note that Novara Arch is dividing the study area in two distinct depocenters. B. Isochore map of the studied interval, representing the total TWT thickness of the seismic sequences OL1 to Mi6. C. Strike oriented 2D line showing the internal morphology of the Novara Arch, stratigraphic elements are after Tindale et al. (1998). P1: Pyrenees-1, M1: Macedon-1, M3: Macedon-3, R1: Ramillies-1. Data courtesy of PGS.

accumulated under semi-arid conditions in Cape Range area (Collins et al., 2006). Following this emersion event, the ramp evolved into a rimmed platform, characterised by the presence of geomorphic barriers observed from 2D seismic reflection profiles in the Carnarvon Basin (Cathro et al., 2003; Romine and Durrant, 1996; Ryan et al., 2007; Young et al., 2001). The barrier structures belong to the middle Miocene seismic reef track that developed along most of the NWS during the middle Miocene (McCaffrey et al., 2020), and possibly as far south as the Great Australian Bight (Feary and James, 1995; O'Connell et al., 2012). They are time-equivalent to lagoonal deposits rich in corals and other tropical organisms that outcrop in Cape Range anticline (Riera et al., 2021). Siliciclastic influx re-established during the late middle Miocene, leading to the accumulation of the mixed dolomite, limestones and siliciclastic Bare Formation and Pilgramunna Formation (Condon et al., 1955; Heath and Apthorpe, 1984; Hocking et al., 1987). The seismic character of those siliciclastic deposits is known from the Dampier sub-basin, directly north of the Barrow sub-basin, where they form delta and sandbars developed on a karstified surface (Sanchez et al., 2012a; Tagliaro et al., 2018).

3. Data and methods

3.1. Seismic datasets

Regional seismic interpretation was conducted on a 3D seismic volume extracted from the PGS Carnarvon MegaSurvey covering an area of 11,008 km^2 with a spatial resolution of 50 m × 50 m, and a vertical sampling rate of 4 ms (Fig. 1). Analysis was performed on this extracted volume to reduce computation time and to focus the investigation on the offshore area in the vicinity of Cape Range anticline (i.e., North West Cape). A full-volume seismic interpretation workflow (Paumard et al., 2019a), including the creation of a relative geological time model and the extraction of 100 3D seismic horizons, was conducted using PalaeoScan™ software. Key seismic stratigraphic surfaces (i.e., seismic unconformities, *sensu* Mitchum et al., 1977a) were identified based on strata terminations (Mitchum et al., 1977b; Posamentier et al., 2022).

3.2. Offshore wells

The investigated area overlaps with multiple exploration wells targeting the Mesozoic reservoirs of the Exmouth-Barrow sub-basins. While the Miocene interval is not cored in this area, it is locally sampled in the form of well cuttings or, more occasionally, side-wall-cores. Four offshore exploration wells, Macedon-1, Macedon-3, Ramillies-1 and Pyrenees-1, were identified as valuable for this study (Fig. 1). Age dating mainly relies on biostratigraphic data published in well completion reports (Rexilius and Powell, 1994a, 1994b; Table 1). It must be noted that regional age dating of the Oligo-Miocene strata of the NWS mainly relies on biostratigraphy of planktic foraminifera (i.e., N-zones classification from Blow, 1969) that can be correlated with absolute ages following Wade et al. (2011). As such, planktic foraminiferal zones are also followed in this study (Fig. 3).

One hundred and thirty-three thin sections of selected well cuttings and side-wall-cores were examined in transmitted light with a petrographic microscope. Petrographic descriptions of carbonate facies follow the nomenclature from Dunham (1962) to describe depositional texture and fabric, while description of quartz grain grades, sphericity and sorting follow respectively Wentworth (1922), Powers (1953) and Pettijohn et al. (1972). In parallel to the published petrographic descriptions, ages based on published biostratigraphy were reassessed using the observation of foraminifera through thin sections and strontium ($^{87}Sr/^{86}Sr$) isotopic age dating (Table 1). A whole-rock analysis method was applied to compare with other studies of the Miocene strata of the NWS (e.g., Rosleff-Soerensen et al., 2012, 2016; Thronberens et al., 2022). Measured ratios are presented in Table 1. For isotopic sampling, material was first examined with a low-power binocular microscope in reflected light, and matrix subsamples were taken with a dental drill, avoiding coarse cements where present. This method is particularly suitable in dating micropackstone, which is less cemented than the other rocks, and which are abundant in offshore wells. All samples were dissolved in 1 M acetic acid to minimise extraction of strontium from clays and other terrigenous materials (DePaolo et al., 1983), and strontium extraction followed standard methods of ion exchange. The isotopic compositions were measured on a VG 354 thermal ionisation mass. External precision estimated by routine analysis of the NBS987 87 Sr/86 Sr standard over the period of analysis was ±0.000018. Data are normalised to NBS987 87 Sr/86 Sr = 0.710235. Isotopic age determination is based on the strontium seawater curve of McArthur and Howarth (2005) calibrated to the timescales of Gradstein et al. (2005; Version 4: 08/03). Although quantifying strontium age error is imprecise, previous large-scale whole-rock studies such as Allan et al. (2000) and van Buchem et al. (2010) indicate that, excluding larger localised outliers, age error caused by uncertainties in the seawater curve, analytical uncertainty and isotopic heterogeneity in the samples can be in the order of ±0.5 Ma to 1.0 Ma. Consistency between strontium isotopic age and available biostratigraphic data was systematically checked, to identify potentially erroneous values.

3.3. Outcrops

Outcrops of Miocene marine strata are restricted to three locations, all within the southernmost portion of the NWS: (1) Cape Range anticline, (2) Giralia Range anticline, and (3) Barrow Island. Stratigraphy of the Miocene outcrops from Cape Range anticline - including naming and dating of the Mandu Limestone/Calcarenite, Tulki Limestone, Trealla Limestone and Pilgramunna Formation - was defined during regional state-funded geological campaigns in the 1950's (Condon et al., 1955, 1953; Crespin, 1955). Subsequent published studies are few, and include geological mapping (van de Graaff et al., 1982, 1980), regional stratigraphic reviews (Hocking et al., 1987), biostratigraphy (Chaproniere, 1977, 1975; Riera et al., 2019b), field sedimentology (Collins et al., 2006; Riera et al., 2022, 2021) as well as diagenetic evolution and petrophysical properties (Matonti et al., 2021). Published descriptions of onshore cores, which were collected in Cape Range anticline either for oil and gas exploration or quarrying, also contain sedimentological and biostratigraphic information on the Miocene strata present onshore (Apthorpe, 1965; Chaproniere, 1976; Riera et al., 2019b). Along Barrow Island, Miocene outcrops are exclusively represented by the Trealla Limestone, which is designated as Poivre Formation there (Hickman and Strong, 2003; McNamara and Kendrick, 1994). Miocene rocks present in the Giralia Range anticline are restricted to the Trealla Limestone that forms low-lying outcrops (Haig et al., 2020; van de Graaff et al., 1980).

Outcrops investigated in this study are exclusively from Cape Range anticline (Figs. 1, 4). Outcrops were examined during three field trips conducted in Cape Range anticline between October 2015 and July 2017. They include outcrops 10's of metres thick and several kilometres long (i.e., Pilgonaman Gorge, Shothole Canyon, the unnamed canyon north of Badjirrajirra Creek), low-lying metre-scale outcrops (i.e., north Water Corporation Land, Mount Lefroy) and quarries (i.e., from Mowbowra Creek area). Results of these field campaigns are published (Riera et al., 2019b, 2021, 2022), but no integration of the entire Miocene succession has been completed yet. Age dating of outcrops is based on published studies (Chaproniere, 1977, 1975; Crespin, 1955; Haig et al., 2020; Riera et al., 2019b, 2021, 2022) complemented with strontium isotopic dating and foraminiferal biostratigraphy, following the methods used to date the offshore wells.

Table 1
Stratigraphic markers in the offshore wells Ramillies-1, Macedon-1, Macedon-3 and Pyrenees-1. Information is either coming from well completion reports (Rexilius and Powell, 1994a, 1994b), from biostratigraphic observations made during this study or from strontium isotope analysis.

Strontium isotope analysis

Sample name	Norm ratio	Error % 2SEM	McArthur 04 age (±1 Ma)
Ramillies-1 1025 mKB	0.708636	0.0013	17.2
Ramillies-1 1250 mKB	0.70837	0.0013	21
Ramillies-1 1250 mKB #2	0.708382	0.0013	20.8
Ramillies-1 1525 mKB	0.708095	0.0015	26.5
Ramillies-1 810 mKB	0.708832	0.0014	11.5
Macedon-1 445 mKB	0.708776	0.0011	14.8
Macedon-1 455 mKB	0.70863	0.0013	17.3
Macedon-1 465 mKB	0.708627	0.0011	17.4
Macedon-1 505 mKB	0.708545	0.0014	18.4
Macedon-1 545 mKB	0.708496	0.0015	19
Macedon-1 575 mKB	0.708476	0.0012	19.3
Macedon-1 595 mKB	0.708477	0.0015	19.3
Macedon-1 655 mKB	0.70846	0.0014	19.5
Macedon-1 675 mKB	0.708427	0.0013	20
Macedon-1 787.5 mKB	0.708107	0.0013	26

Biostratigraphy

Well name	Cutting depth interval (mKB)		Foraminiferal zone	Source	Foraminifera identified (this study)
Ramillies-1	810	820	Tf1–Tf2 stage (no younger than 13 Ma)	This study	*Flosculinella* sp.
Macedon-1	270	270	Zones N21/N20	Rexilius and Powell, 1994a	
Macedon-1	290	290	Zone N19	Rexilius and Powell, 1994a	
Macedon-1	310	375	Zone N18	Rexilius and Powell, 1994a	
Macedon-1	385	385	Zone N17A or younger	Rexilius and Powell, 1994a	
Macedon-1	393	415	Indeterminate	Rexilius and Powell, 1994a	
Macedon-1	425	425	Zone N9	Rexilius and Powell, 1994a	
Macedon-1	435	435	Zones N9/N8	Rexilius and Powell, 1994a	
Macedon-1	445	465	Zone N8	Rexilius and Powell, 1994a	
Macedon-1	475	475	Zone N7 or younger	Rexilius and Powell, 1994a	
Macedon-1	485	485	Indeterminate	Rexilius and Powell, 1994a	
Macedon-1	495	545	Zones N7/N6	Rexilius and Powell, 1994a	
Macedon-1	555	635	Zones N5/N4	Rexilius and Powell, 1994a	
Macedon-1	655	775	Zone N4	Rexilius and Powell, 1994a	
Macedon-1	785	785	N3?	Rexilius and Powell, 1994a	
Macedon-1	787.5	787.5	Zone P5 or younger	Rexilius and Powell, 1994a	
Macedon-1	791	803	Zone P4	Rexilius and Powell, 1994a	
Pyrenees-1	637	643	Zone N9	This study	*Praeorbulina glomerosa* + *Orbulina suturalis*
Pyrenees-1	668	668	Zone N8/N9	This study	
Pyrenees-1	689	723	Zone N8	This study	*Praeorbulina glomerosa*
Pyrenees-1	740	740	Zone N8	This study	*Praeorbulina glomerosa*
Pyrenees-1	750	750	Zone N8	Rexilius and Powell, 1994b	
Pyrenees-1	757.5	805	Zones N7/N6	Rexilius and Powell, 1994b	
Pyrenees-1	810	810	Indeterminate	Rexilius and Powell, 1994b	
Pyrenees-1	822.5	880	Zones N6–N4	Rexilius and Powell, 1994b	
Pyrenees-1	884	884	Zone N4	Rexilius and Powell, 1994b	
Pyrenees-1	892.5	895	Zone N3	Rexilius and Powell, 1994b	
Pyrenees-1	897.5	897.5	Zones P14/P13	Rexilius and Powell, 1994b	
Pyrenees-1	900	900	Zone P12	Rexilius and Powell, 1994b	
Pyrenees-1	902.5	905.5	Zones P6/P5	Rexilius and Powell, 1994b	
Macedon-3	397	397	Miocene	This study	*Lepidocyclina Nephrolepidina*
Macedon-3	410	410	Miocene	This study	*Lepidocyclina* sp.

4. Seismic stratigraphic framework

Eight regional seismic unconformities were identified in the Exmouth-Barrow sub-basins, bounding seven seismic sequences (Figs. 3, 5, 6).

4.1. Seismic reflector SR0

Regional reflector SR0 is a surface of nondeposition (i.e., hiatus) overlying the Palaeocene to lower Eocene strata. It marks the base of the late Oligocene to Miocene cycle of sedimentation (Fig. 5). The hiatus is not total, and there is locally a thin middle Eocene-lower Oligocene layer (i.e., ~8 m thick) in the Southern depocenter (see Pyrenees-1 897.5 mKB in Table 1). Thus, the horizon can be interpreted as a condensed marine surface (maximum flooding) associated with very low sedimentation rates. SR0 is either overlain by distal downlap of late Oligocene strata, or by basin sub-parallel high-amplitude seismic reflectors of Miocene age where Oligocene deposits are absent (Fig. 5). Analysis of offshore well cuttings indicates that the reflector SR0 formed between the base of the planktic foraminiferal zone N3 and the top of the zone N4 (see Macedon-1 785 mKB/775 mKB and Pyrennes1 892.5 mKB, Table 1, Fig. 6). Strontium isotope analysis further indicates an age range between 26 ± 1 Ma and 26.5 ± 1 Ma (Macedon-1 787.5 mKB; Ramillies-1 1525 mKB; Table 1), which is used for this study (Fig. 3).

4.2. Seismic reflector SR1

Reflector SR1 is a high-amplitude seismic reflector which marks the top of the seismic sequence OL1. This reflector is marked by the presence of both onlap and downlap of the seismic sequence Mi1 above (Fig. 5). Analysis of well cuttings indicates that the seismic reflector

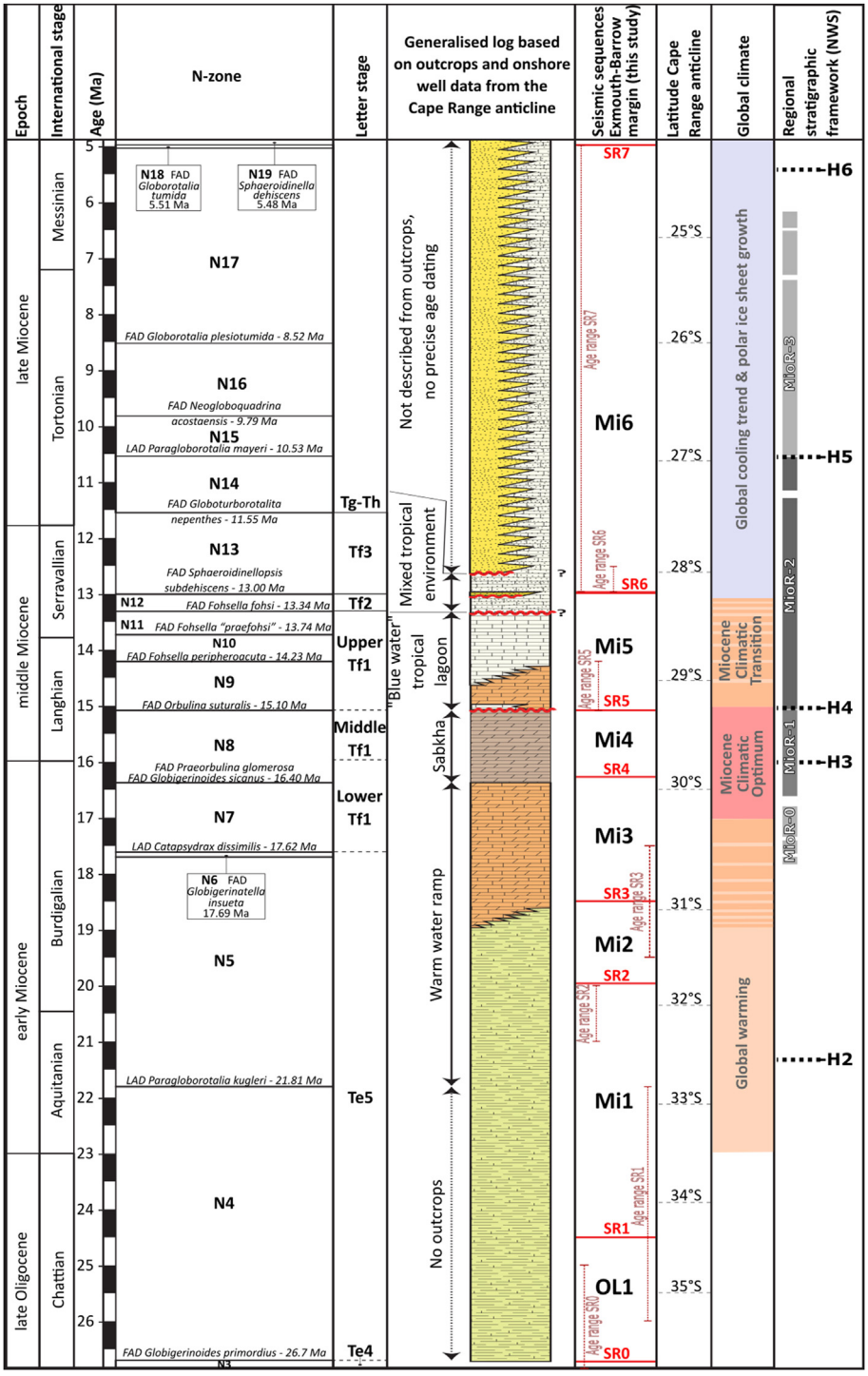

Fig. 3. Generalised stratigraphic column of the study area, compared to absolute ages, international stages (Cohen et al., 2018), N-zones (Blow, 1969), Australasian "letter-stages" (BouDagher-Fadel, 2018), outcrops (this study and Riera et al., 2019b, 2021, 2022), regional seismic sequences along the Exmouth-Barrow margin (this study), latitude of Cape Range anticline (after Seton et al., 2012 in the application GPlate from Müller et al., 2018), global climate (summarised from Flower and Kennett, 1994; Mudelsee et al., 2014; Sangiorgi et al., 2018; Zachos et al., 2001) and regional stratigraphic framework of the Australian North West Shelf (after McCaffrey et al., 2020).

SR1 formed during the foraminiferal zone N4 (i.e., 21.84–26.7 Ma; Pyrenees-1 822.5–880 mKB, Macedon-1 655–775 mKB). This age is supported by strontium isotope analysis, which indicates a deposition of the sediment between 20 Ma and 26 Ma (see Macedon-1 675 mKB, Macedon-1 787.5 mKB, Ramillies-1 1250 mKB and Ramillies-1 1525 mKB, Table 1, Fig. 6). The age range of the reflector SR1 is then estimated between 21.81 Ma and 26 Ma (Fig. 3).

4.3. Seismic reflector SR2

Regional reflector SR2 marks the top of the seismic sequence Mi1. This reflector is marked by the presence of both onlap and downlap of the seismic sequence Mi2 above (Fig. 5). Strontium isotope analysis of cuttings from Macedon-1 675 mKB and Ramillies-1 1250 mKB indicates an age of this reflector between 20 ± 1 Ma and 20.8 ± 1 Ma (Fig. 3; Table 2).

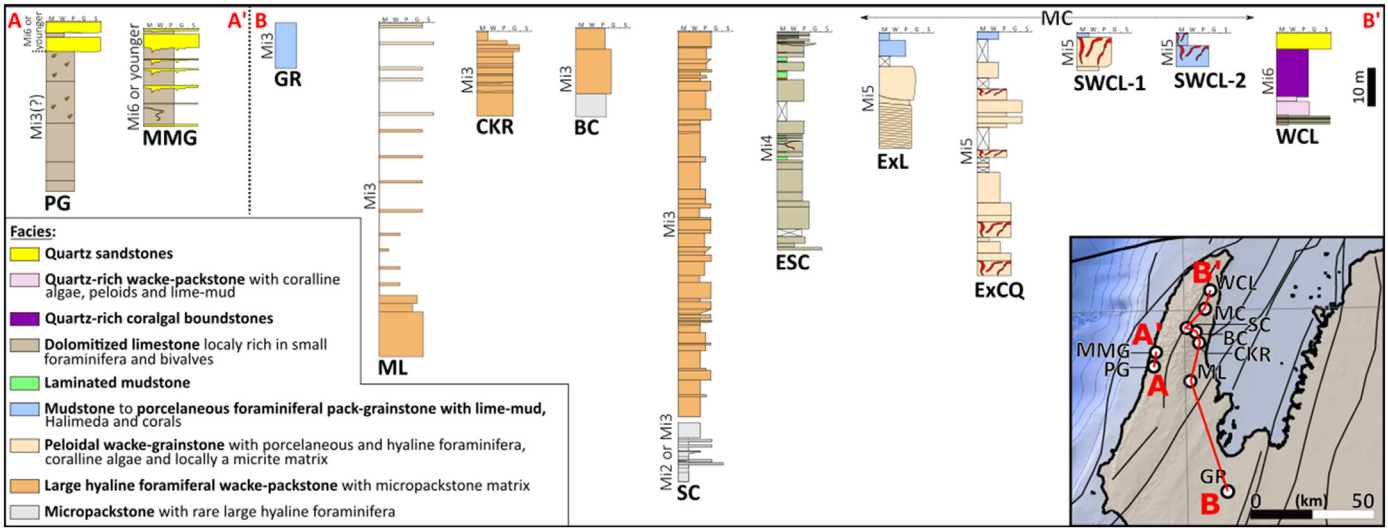

Fig. 4. Simplified lithostratigraphic columns of the Miocene outcrops. PG: Pilgonaman Gorge, MMG: Mandu Mandu Gorge, GR: Giralia Range, ML: Mount Lefroy, CKR: Charles Knives Road, BC: unnamed canyon north of Badjirrajirra Creek, SC: Shothole Canyon, ESC: entrance Shothole Canyon, MC: Mowbowra Creek, WCL: Water Corporation Land.

4.4. Seismic reflector SR3

Regional reflector SR3 marks the top of the seismic sequence Mi2. SR3 is marked by both onlap and downlap of the seismic sequence Mi3 above (Fig. 5). Strontium isotope analysis from the cuttings of Macedon-1 indicates that the surface SR3 has an age of 18.5 ± 1 Ma. This age is consistent with well completion reports from Macedon-1 and Pyrenees-1 which give an age interval between foraminiferal zones N4 and N7 (Table 2). Hence, the age of SR3 is considered as 18.5 ± 1 Ma (Fig. 3).

4.5. Seismic reflector SR4

Seismic reflector SR4 is a regional surface which marks the top of the seismic sequence Mi3. This regional surface is either overlying truncations, possibly representing a karstified surface, or is represented by the presence of onlap from the sequence Mi4 above (Fig. 5). Strontium isotope analysis of well cuttings from Ramillies-1 indicates an age between 21 ± 1 Ma and 17.2 ± 1 Ma (see Ramillies-1 1250 mKB and 1025 mKB; Table 1). This age range is supported by biostratigraphy and strontium isotopes in Macedon-1, which give an age range between 18.4 ± 1 Ma (Macedon-1 505 mKB; Table 1) and 17.4 ± 1 Ma (Macedon-1 465 mKB; Table 1), or between the foraminiferal zones N6 and N8 (Macedon-1 545–445 mKB; Table 1). Additionally, the presence of *Praeorbulina glomerosa* (recognisable by their thick and coarsely cancellate wall, final chamber well enveloping the earlier chambers and apertures confined to the suture) in strata below and above SR4 in the well Pyrenees-1 (689 mKB – 740 m mKB; Table 1) indicates that the reflector falls within the N8 planktic foraminiferal zone, and that it is no older than 16.29 Ma (Wade et al., 2011). It is then considered that this surface was formed around ~16.3 Ma (i.e., in the upper range of strontium isotope ages; Fig. 3).

4.6. Seismic reflector SR5

Seismic reflector SR5 is a regional surface which marks the top of seismic sequence Mi4. SR5 is marked by the presence of downlapping reflectors from sequence Mi5 on sequence Mi4, which is locally truncated (Fig. 5). Age dating based on published well completion reports indicates that the reflector SR5 was formed in the N9/N8 zone (i.e., between 14.23 Ma and 16.40 Ma, see Macedon-1 435–465 mKB; Table 1).

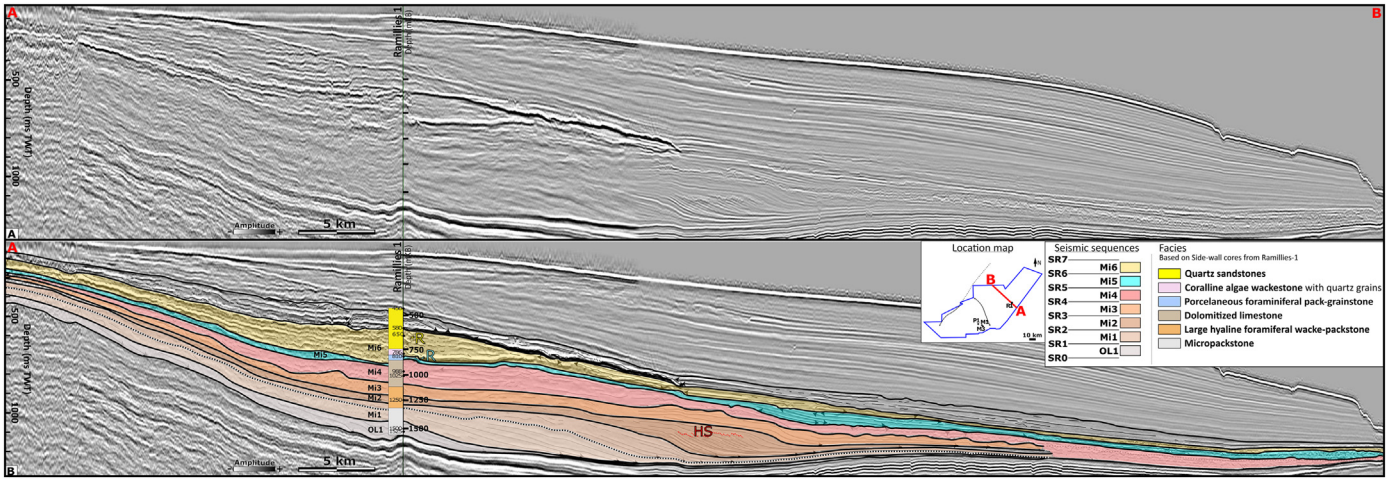

Fig. 5. Un-interpreted (A) and interpreted (B) dip-oriented 2D seismic line in the Northern depocenter cross-cutting well Ramillies-1. Note stratal termination of the reflectors and location of well cuttings used for dating. Location of 2D line is indicated in red in the white panel, in the top right corner. R: Ridge, HS: time-transgressive Honeycomb Structure. Data courtesy of PGS.

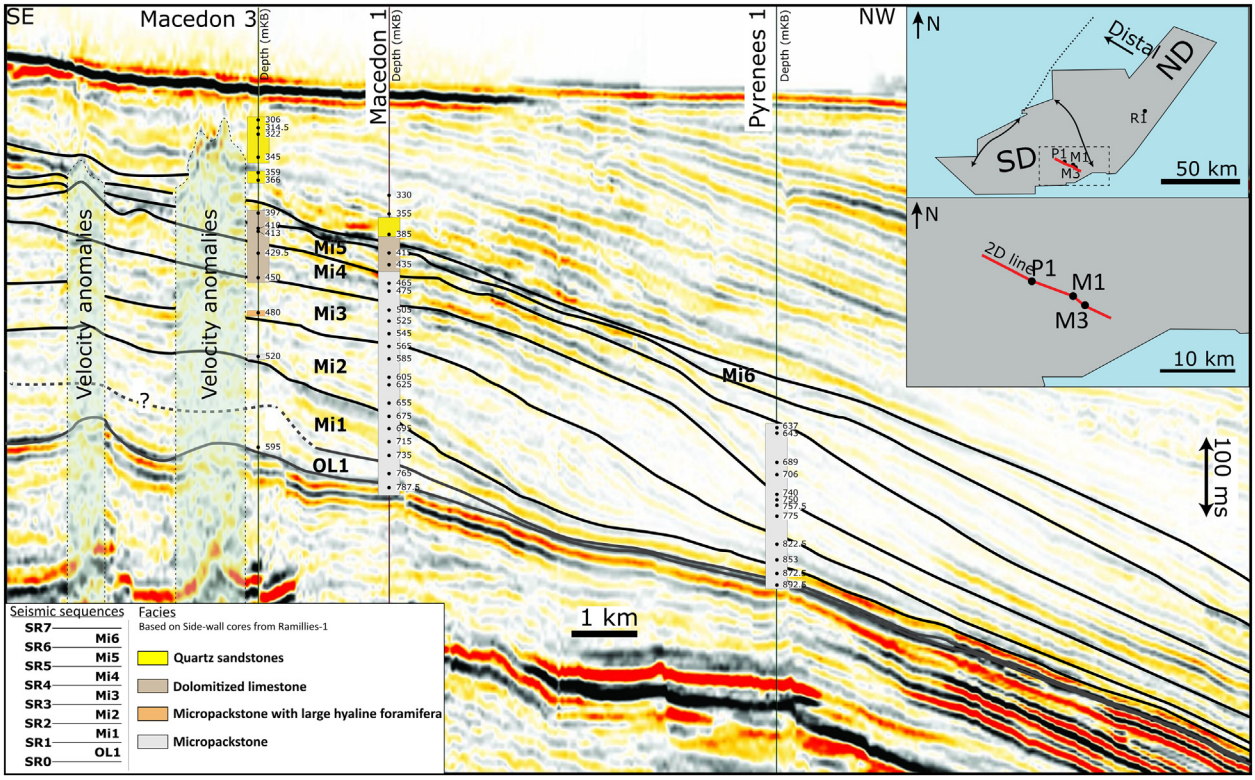

Fig. 6. Interpreted dip-oriented 2D seismic line in the Northern depocenter cross-cutting wells Macedon-3, Macedon-1 and Pyrenees-1. Data courtesy of PGS.

However, the identification of *Orbulina suturalis* and *Praeorbulina glomerosa* at this reflector in Pyrenees-1 (i.e., at 637 mKB; Table 1) supports a formation within the N9 zone (i.e., 14.23 Ma – 15.10 Ma), while the absence of identification of *Orbulina* sp. in deeper cuttings may indicate that SR5 marks the base of the N9 zone. Strontium isotope analysis in Macedon-1 indicates a formation between 14.8 ± 1 Ma and 17.3 ± 1 Ma (respectively from Macedon-1 445 mKB and Macedon-1 455 mKB; Table 1) and between 11.5 ± 1 Ma and 17.2 ± 1 Ma in Ramillies-1 (respectively from Ramillies-1 810 mKB and Ramillies-1 1025 mKB; Table 1). Hence, it is considered that SR5 could have formed anytime within the N9 zone (i.e., 14.23 Ma – 15.10 Ma; Fig. 3).

4.7. Seismic reflector SR6

Seismic reflector SR6 is a regional truncation surface (Fig. 5). Cuttings from the upper part of sequence Mi5 and younger strata are not available in Pyrenees-1, but it is possible to deduce from underlying cuttings that the interval is younger than the base of the foraminiferal zone N9 (i.e., 15.10 Ma, Pyrenees-1 637 mKB, Table 1). Biostratigraphy from Macedon-1 indicates that the reflector SR6 was formed between the foraminiferal zones N9 and N17/N18 (i.e., 15.10–5.48 Ma, Macedon-1 385 mKB and 425 mKB; Table 1). The presence of *Lepidocyclina* (*Nephrolepidina*) above reflector SR6 in Macedon-3 (Macedon-3 397 mKB, Table 1) further supports a formation during the Miocene, even if *Lepidocyclina* (*Nephrolepidina*) may still be locally extant during the lower Pliocene (BouDagher-Fadel, 2018). Observation of *Flosculinella* sp. in the cutting 810–820 mKB from Ramillies-1, which is located just below the reflector SR6, indicates an age no younger than 13 Ma (based on BouDagher-Fadel, 2018; Table 1). Strontium isotope analysis of a SWC from Ramillies-1 collected at 810 mKB indicates an age of 11.5 ± 1 Ma (Table 1), hence slightly younger than the biostratigraphic age range. Thus, the age of this reflector is considered to be ~13 Ma to 12.5 Ma.

4.8. Seismic reflector SR7

Seismic reflector SR7 is a high-amplitude reflector locally forming a truncation surface (Fig. 5). It is locally overlaid by downlapping strata. Reflector SR7 could not be dated. However, the reflector is located below strata belonging to the N18 zone, and hence is older than 5.48 Ma (see Macedon-1 310–375 mKB; Table 1). Hence, reflector SR7 could have formed anytime between 5.48 Ma and 13 Ma (i.e., maximum possible age of SR6; Fig. 3).

5. Stratigraphic evolution of the Exmouth-Barrow margin

5.1. Late Oligocene - early Miocene

The late Oligocene-early Miocene deposits are represented by four seismic sequences along the Exmouth-Barrow margin, namely OL1, Mi1, Mi2 and Mi3 (Figs. 3, 5, Table 2). The sequence OL1 is composed of linear parallel clinoforms prograding towards the northwest on Palaeogene and Eocene strata (Fig. 5). This depositional sequence is only observed in the eastern part of the Northern depocenter, and is absent from the Southern depocenter (Figs. 7, 8). Cuttings from offshore well Ramillies-1 show that the sequence OL1 is formed by marly micropackstone, with scarce quartz grains, scarce planktic foraminifera, scarce small hyaline foraminifera and biogenic debris (Fig. 9D). The matrix is composed of micrite and micropackstone. There is no observed variation in sedimentary facies along the depositional profile, however, strata are locally dolomitized or recrystallised. No notable geomorphologies were observed in this sequence, except for linear and closely spaced headless gullies on clinoform foresets in the northern depocenter (Fig. 10A). The gullies have a run-out distance of ~3 km to 4 km, a width of ~80 m, and the distance between two gullies range from ~300 m to ~500 m.

Seismic sequence Mi1 is composed of sigmoidal-to-linear parallel clinoforms prograding on top of the seismic sequence OL1. Mi1 is

Table 2
Summary of the main characteristics of the seven seismic sequences and time-equivalent outcrops described along the Exmouth-Barrow margin.

Seismic sequence	Regional reflectors	Age basal reflector (Ma)	Margin morphology	Seismic geomorphologies observed	Proximal part sequence	Distal part	Outcrops in Cape Range anticline
	SR7	No younger than 5.48 Ma	/	/	/	/	/
Mi6	SR6	~13 Ma or younger	Chaotic to subparallel reflectors dapped over Mi5	Curvi-linear ridge	Quartz sandstone	NA	Top: quartz sandstones: siliciclastic beach and soil deposits Base: quartz-rich limestones with coralline algae and metre-scale globose corals interlayer with coarse quartz sandstones: coralgal factory in mixed carbonate-siliciclastic environment
Mi5	SR5	15.10–14.23 Ma	Chaotic, subparallel and convergeant reflectors dapped over Mi4	Ridge (mid-platform), slope channels (distal)	Dolomitized foraminiferal pack-grainstone	NA	Coral-rich floatstone, mudstone, wackestone and packstone with larger foraminifera and peloids: tropical blue-water lagoon
Mi4	SR4	~16.3 Ma	Chaotic to subparallel reflectors dapped over Mi3	Mass Transport Complexes, channels	Dolomitized foraminiferal wackestone, microcrystalline dolomite	Micropackstone with dolomite rhombs	Partially dolomitized bivalve rudstone, mudstone with gastropods and banded mudstone of inferred microbial origin: fossil sabkha
Mi3	SR3	18.5 Ma ± 1 Ma	Sigmoidal clinoforms	Mass Transport Complex	Micropackstone with *Cycloclypeus* sp. and *Lepidocyclina* (*Nephrolepidina*) sp. or dolomite (upper topsets)	Marly micropackstone	Shallower facies: wackestone to grainstone with *Cycloclypeus* sp., *Lepidocyclina* sp., *Operculina* sp., *Sorites* sp., *Austrotrillina* sp., *Flosculinella* sp. and coralline algae: ramp (mesophotic zone) Deeper facies: silty micropackstone and foraminiferal rudstone, wackestone and packstone with *Cycloclypeus* sp., *Lepidocyclina* sp. and *Operculina* sp.: ramp (oligophotic zone)
Mi2	SR2	20.5 Ma ± 1.5 Ma	Sigmoidal clinoforms	Smooth clinoform fronts, time-transgressive honeycomb structure	Micropackstone with *Cycloclypeus* sp., *Lepidocyclina* (*Nephrolepidina*) sp. and *Operculina* sp.	Marly micropackstone	Silty micropackstone and foraminiferal rudstone, wackestone and packstone with *Cycloclypeus* sp., *Lepidocyclina* sp. and *Operculina* sp.: ramp (oligophotic zone)
Mi1	SR1	22 ± 2 Ma	Sigmoidal to linear clinoforms	Smooth clinoform fronts	Marly micropackstone with reworked *Cycloclypeus* sp.	Marly micropackstone	NA
OL1	SR0	26 Ma ± 1 Ma	Linear clinoforms	Linear and closely spaced headless gullies on clinoform foresets	Marly micropackstone	Marly micropackstone	NA

mainly observed in the eastern part of the Northern depocenter, while its upper part is also present in the eastern part of the Novara Arch area and southern depocenter, where it is represented by very thin clinoform bottomsets (Fig. 7). Cuttings from offshore well Macedon-1 show that clinoform foresets are composed of marly micropackstone with micrite (Fig. 9E–F). Cutting analysis from Ramillies-1 further indicates that the clinoform topsets are organised in a shallowing-upward sequence with: (1) marly micropackstone in the lower and more distal part of the topsets; and (2) marly micropackstone with reworked *Cycloclypeus* sp. and undifferentiated skeletal debris of in the upper and proximal part of the topsets. Strata are locally dolomitized.

Seismic sequence Mi2 displays sigmoidal clinoforms prograding above Mi1. Similar to the underlying sequences (i.e., OL1, Mi1 and Mi1), Mi2 reaches its maximum time-thickness (~150 ms) in the Northern depocenter (Fig. 7). Cutting analysis from offshore well Ramillies-1 indicates that the more distal part of the topsets are composed of micropackstone with *Cycloclypeus* sp., *Lepidocyclina* (*Nephrolepidina*) sp. and *Operculina* sp. (Ramillies-1 1250 mKB, Fig. 9G). Cuttings from offshore well Pyrenees-1 indicate that the clinoform bottomsets are composed of marly micropackstone (Pyrenees-1 822.5 mKB, Fig. 9H). The only geomorphology observed in this sequence is a time-transgressive honeycomb structure of inferred diagenetic origin, which is locally present at the clinoform topset-to-foreset transition (Figs. 5, 10B; Riera et al., 2019a).

The seismic sequence Mi3 is composed of sigmoidal clinoforms with a progradational and aggradational pattern, which present comparable thickness in both the topset and bottomset domains (i.e., ~100 ms, Fig. 5). Mi3 is present in the proximal parts of both the Northern and Southern depocenters (Figs. 7, 8), and its upper part is eroded. Cutting analysis from offshore wells Ramillies-1 and Macedon-3 indicates that the distal part of the topsets are composed of micropackstone with *Cycloclypeus* sp. and *Lepidocyclina* (*Nephrolepidina*) sp. (Macedon-3 480 mKB, Fig. 9I). The uppermost part of the topsets is dolomitized. Cuttings from offshore well Pyrenees-1 indicate that the bottomsets are composed of marly micropackstone, which suggests an accumulation in a deep area, without photic organisms (i.e., aphotic zone). A very large Mass Transport Complex (MTC) with a headwall scarp at least 24 km wide and a runoff distance of at least 40 km is present in the upper part of the sequence in the Northern depocenter (Fig. 10C). This MTC reworks underlying bottomsets of the sequences OL1, Mi1 and Mi2 and the lower part of MI3. The MTC headwall scarp is superimposed on a fault which itself crosscuts Cretaceous to early Miocene strata (Fig. 10D).

Seismic sequences Mi2 and Mi3 outcrop in the eastern part of Cape Range anticline (Fig. 4). The most spectacular outcrops form shallowing-upward sequences along the flanks of canyons several kilometres long and tens of metres deep, and are accessible from the Shothole Canyon, Badjirrajirra Creek and Charles Knife Road (Fig. 9A–B). Detailed description of these outcrops is presented in Collins et al.

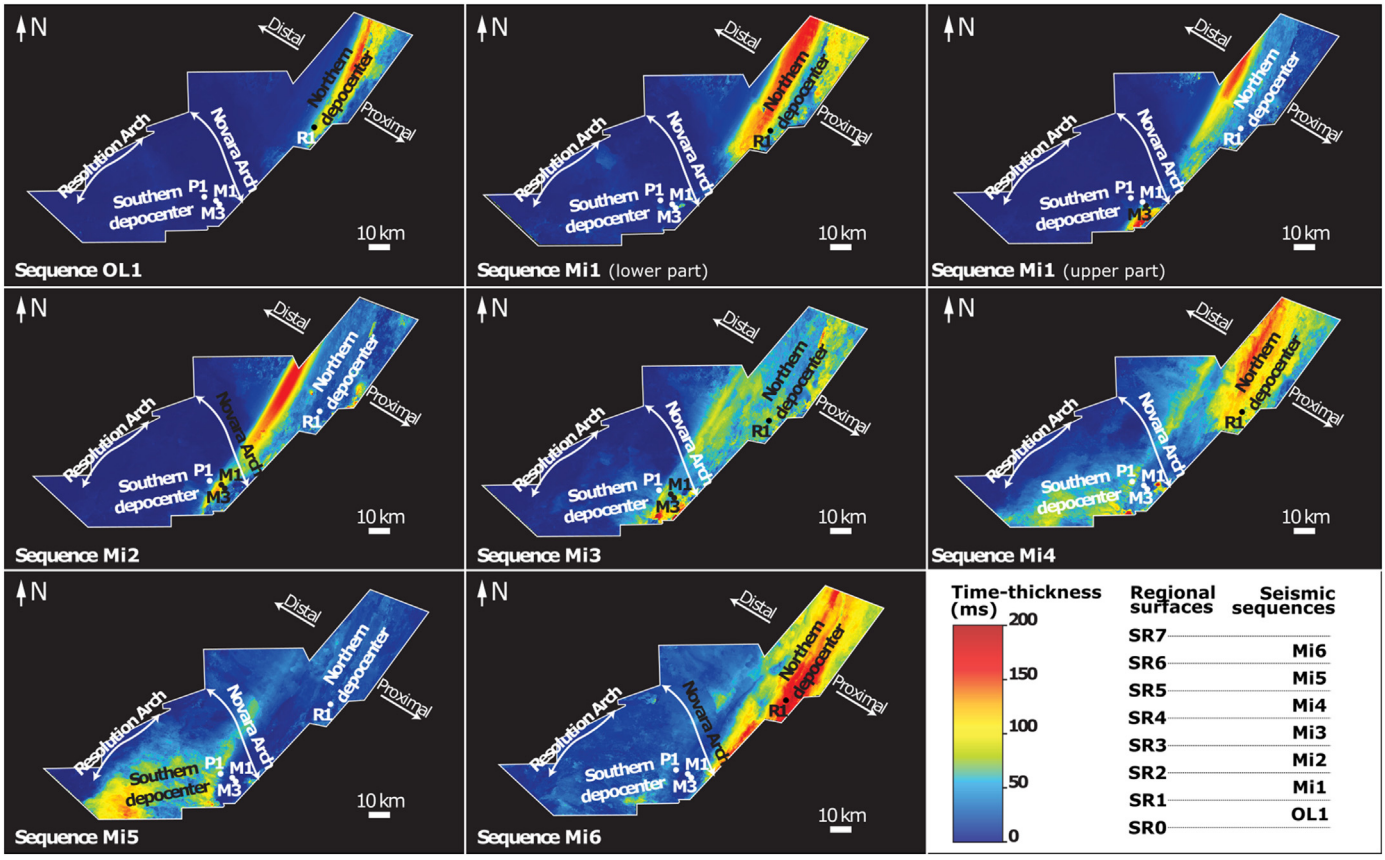

Fig. 7. Isochore maps presenting variations in time-thickness (ms TWT) of different seismic sequences; red areas represent locations of maximum sediment accumulation. Note change in the style of sediment accumulation between the sequences OL1-Mi2 (i.e., maximum accumulation is on prograding clinoform forsets) and the sequences Mi3-Mi6 (maximum accumulation on retrograding topsets and on bottomsets). P1: Pyrenees-1, M1: Macedon-1, M3: Macedon-3, R1: Ramillies-1. Data courtesy of PGS.

(2006), Condon et al. (1955), Haig et al. (2020) and Hocking et al. (1987), and their depositional model has been recently updated using outcrop and offshore well data by Riera et al. (2022). The outcrops form a shallowing-upward succession from the north-west to the south-east, with the strata that accumulated at the deepest water depths present at the base of the northern outcrops (i.e., Shothole Canyon and unnamed canyon north of Badjirrajirra Creek; Fig. 1) and the strata that accumulated at shallower water depths present in the upper part of the southern outcrops (i.e., Charles Knife Road and Mount Lefroy). Most outcropping strata contain larger foraminifera (Fig. 9C). Facies follow an apparent light-related zonation, and sediment accumulated in the photic zone along an inferred ramp profile (*sensu* Burchette and Wright, 1992). Deeper and older facies, accumulated in the oligophotic zone (*sensu* Pomar, 2001), are represented by silty micropackstone and foraminiferal rudstone, wackestone and packstone with *Cycloclypeus* sp., *Lepidocyclina* sp. and *Operculina* sp. The shallower early Miocene strata outcropping in Cape Range anticline are foraminiferal wackestone to grainstone with *Cycloclypeus* sp., *Lepidocyclina* sp., *Operculina* sp., *Sorites* sp., *Austrotrillina* sp., *Flosculinella* sp. and coralline algae. No outcrops with very shallow facies, characteristic of the euphotic zone, were observed in the Cape Range anticline, but such outcrops appear to be present in the Giralia Range anticline, where they are represented by miliolid-rich limestone with *Flosculinella* sp., *Austrotrillina* sp. and *Sorites* sp. inferred to have accumulated in a ~10 m deep marginal lagoon with seagrass meadows (Haig et al., 2020) between ~16 Ma and ~19 Ma (i.e., broadly time-equivalent to the seismic sequence Mi3). The dolomitized outcrops present in the western part of Cape Range anticline, represented by the Mandu Mandu Gorge and Pilgonaman Gorge sections here (Fig. 4), could also be equivalent to the sequence Mi3. Indeed, those outcrops have been dated late Early Miocene to early Middle Miocene by Chaproniere (1977), as they possibly contain *Praeorbulina glomerosa*.

5.2. Late Burdigalian – early Langhian

Seismic sequence Mi4 (Table 2) is composed of chaotic to subparallel seismic reflectors draped over Mi3 (Fig. 5). The proximal part of the sequence is more developed in the Northern depocenter, while its distal part is particularly thick in the Southern depocenter (Figs. 7, 8). Cuttings from offshore wells Ramillies-1 and Macedon-1 indicate that the proximal part of the sequence is composed of partially to fully dolomitized foraminiferal packstone (with *Lepidocyclina* and *Amphistegina*) to microcrystalline dolomite (Fig. 11G–H) whereas its distal part is composed of micropackstone with echinoderm debris, planktic foraminifera and dolomite rhombs, and lacking quartz grains (Fig. 11I). Small channels are present in the distal part of the sequence (Fig. 12), but they are not intersected by wells. These channels have an average run-out distance varying between ~10 km and ~20 km, a maximum run-out distance of ~36 km, and individual channels are spaced by 800 m to 3.5 km. Bottomsets are locally reworked by extensive MTCs, particularly around the Novara Arch area (Fig. 12). On seismic sections, the Mi4 sequence generally marks an overall backstep of the shelf-margin position, a trend that had initiated during Mi3 and is more pronounced to the NE of the study area (Figs. 5, 7, 8).

A single outcrop time-equivalent to the sequence Mi4 was identified (Fig. 4). The outcrop, located at the entrance of Shothole Canyon, is ~54 m thick (Figs. 4, 11A–F). This outcrop, which was first described by Collins et al. (2006), is overlying strata with *Globigerinoides sicanus* (Riera et al., 2019b) and it is interpreted to have accumulated during the N8 zone (i.e., between 16.40 Ma and 15.10 Ma; Fig. 3). The outcrop contains an alternation of partially dolomitized and silicified facies

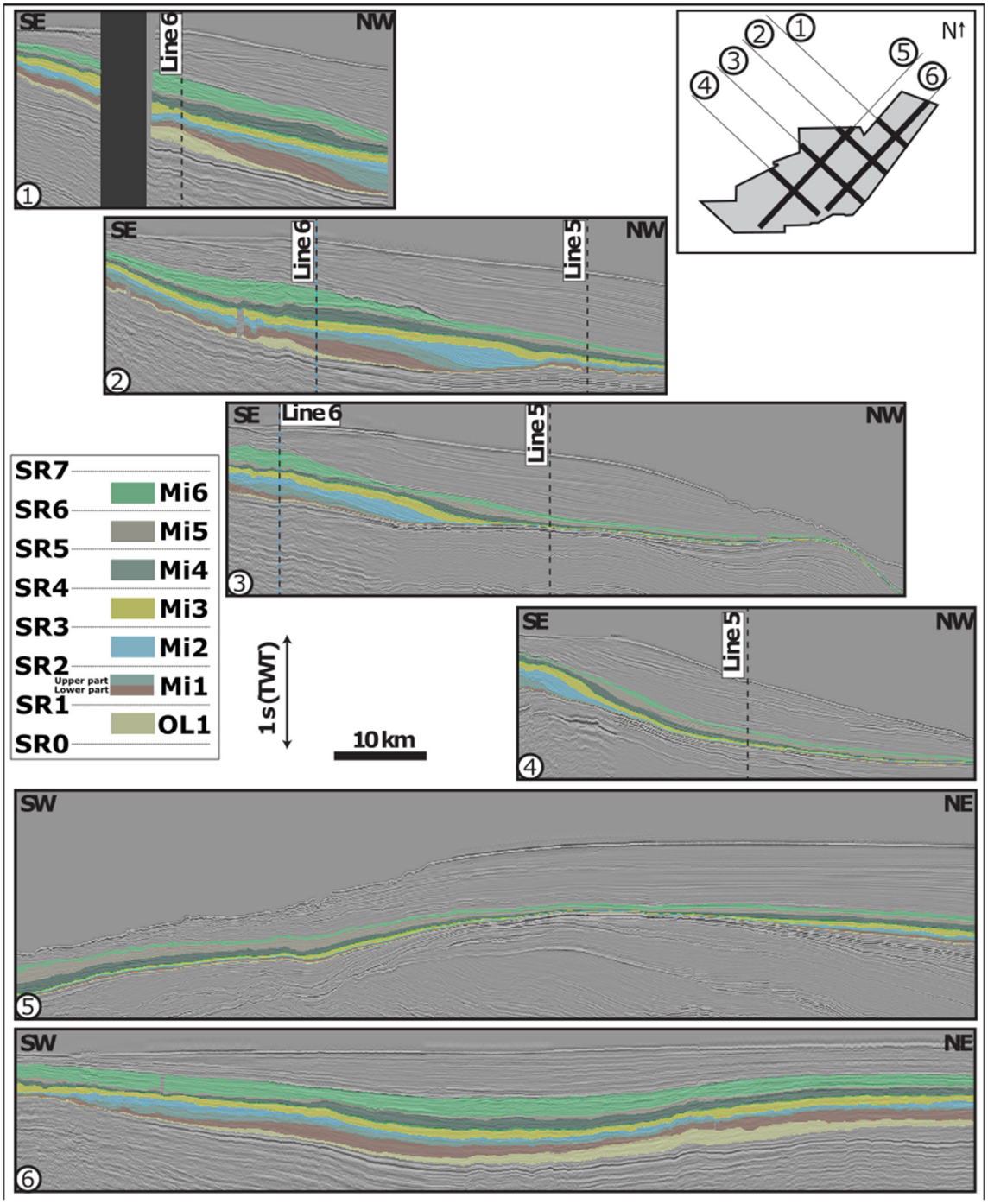

Fig. 8. Strike and dip oriented 2D seismic lines extracted from PGS MegaSurvey showing along-strike variability in thickness in each seismic sequence. Data courtesy of PGS.

organised in sub-horizontal beds. Lithologies can be grouped in bioclast-rich facies, laminated facies and mudstone. Bioclast-rich facies are represented by: (1) patches ~50 cm high and ~50 cm large of very well cemented white to pink mudstone with abundant gastropods and rare broken branching corals (Fig. 11A); and (2) well cemented grey bivalve rudstone (Fig. 11B). The bivalve rudstone contains abundant centimetre-scale moulds of disarticulated bivalves with no preferential orientation, rare gastropod moulds and very rare small (diametre ~3 cm) clypeasteroid echinoderms. Laminated facies consist of finely banded dolomitic mudstone locally silicified, with bands having the width of the outcrops, formed by an alternation of horizontal centimetre-thick beige and white structures (Fig. 11C–D). These structures are locally crinkled and/or form laminated domal and pustular structures (Fig. 11E). Mudstone with polygonal cracks, only present in the upper part of the outcrops (Fig. 11F), are locally intersected by channels with erosional bases which are filled with red sediments interpreted as palaeosols, and clasts of banded deposits.

5.3. Upper Langhian – lower Serravallian

Seismic sequence Mi5 (Table 2) contains sub-parallel to chaotic seismic reflectors draping Mi4 in its proximal part, and convergent reflectors in its distal part. The upper part of the sequence is eroded (Fig. 5). Mi5 is particularly well developed in the distal part of the southern depocenter, where it is up to 200 ms thick (Figs. 7, 8). It is relatively thin in the NE (Fig. 7). Cuttings from offshore well Ramillies-1 indicate

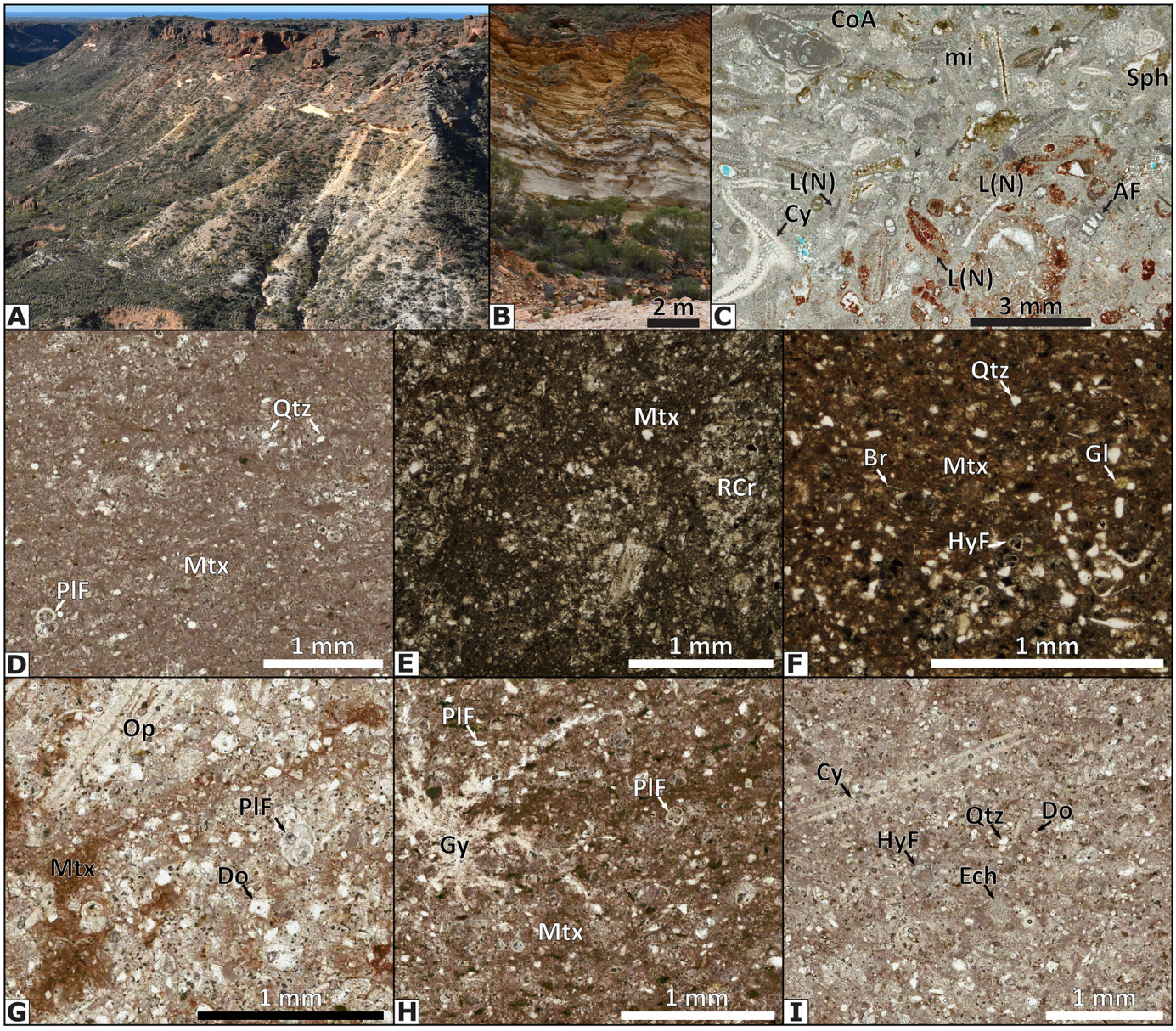

Fig. 9. Field photographs and microphotographs of the ramp outcrops (A–C) and offshore facies (D–I; sequences OL1 to Mi3). A–B. Field photographs illustrating shallowing-upward outcrops present in Cape Range anticline, respectively in Shothole Canyon and an unnamed Canyon north of Badjirrajirra Creek; these outcrops are described in greater detail in Riera et al. (2022). C. Example of facies rich in foraminifera that accumulated in the mesophotic zone (Charles Knife Road, modified from Riera et al. (2022)). D. Marly micropackstone with clayey matrix (Mtx), scarce quartz grains (Qtz) and planktic foraminifera (PlF) observed in clinoform foreset from sequence OL1 (Ramillies-1 1525 mKB). E. Partially recrystallised (RCr) marly micropackstone in topset of sequence Mi1 (Macedon-1 695 mKB). F. Marly micropackstone with scarce quartz grains, scarce glauconitic grains (Gl), rare hyaline foraminifera (HyF) and debris of calcitic organisms (Br) from foreset of sequence Mi1 (Macedon-1 715 mKB). G. Marly micropackstone with rare broken flattened *Operculina* sp. (Op), rare planktic foraminifera (PlF) and rare dolomite rhombs (Do) from proximal topset of sequence Mi2 (Ramillies-1 1250 mKB). H. Marly micropackstone with rare quartz grains, rare planktic foraminifera and a gypsum rosette (Gy) cross-cutting the sediment; cutting is from bottomset of sequence Mi2 (Pyrenees-1 822.5 mKB). I. Marly micropackstone with rare *Cycloclypeus* sp. (Cy), rare quartz grains (Qtz), rare hyaline foraminifera (HyF), rare echinoderm debris (Ech) and rare dolomite rhombs (Do) from topset of seismic sequence Mi3 (Macedon-3 480 mKB).

that the proximal part of the seismic sequence is composed of dolomitized foraminiferal pack-grainstone (Fig. 13F). Two remarkable features are present in the seismic sequence Mi5: (1) a seafloor ridge; and (2) slope channels (Fig. 14). The ridge, which has been first described by Riera et al., (*in press*) is linear. It delineates a lagoon with pinnacles, and has morphological similarities with the modern Australian coastline. It is calibrated by one SWC (Ramillies-1 810 mKB), and is composed of foraminiferal packstone to grainstone with small miliolids, *Sorites* sp., *Amphistegina* sp., and coralline algae (Fig. 13E). The ridge is ~30 m thick based on well data. The sinuous and vertically stacked sub-parallel slope channels are located in the Southern depocenter (Fig. 14A). The channels are ~150 m to 500 m wide and regularly spaced. They have a run-out distance between 30 and 70 km.

This seismic sequence is time-equivalent to outcrops of tropical lagoonal limestone locally rich in corals accumulated in Cape Range anticline area between ~15.10 Ma and ~13.34 Ma. Dating is based on the identification of *Orbulina* sp., *Austrotrillina* sp. and *Flosculinella* sp. (see Riera et al., 2021, 2019b; Figs. 4, 13A–D). These lagoonal limestone outcrop in Mowbowra Creek area, where they are represented by both wackestone and packstone with larger foraminifera and peloids mapped as Tulki Limestone, and by mudstone and coral-rich floatstone mapped as Trealla Limestone (see map from Condon et al., 1955, and facies description by Riera et al., 2021). While outcrops present along creek flanks are extensive, reaching several kilometres in length and a thickness of tens of metres, most of their surface is covered with desert varnish, hence making facies difficult to identify within natural

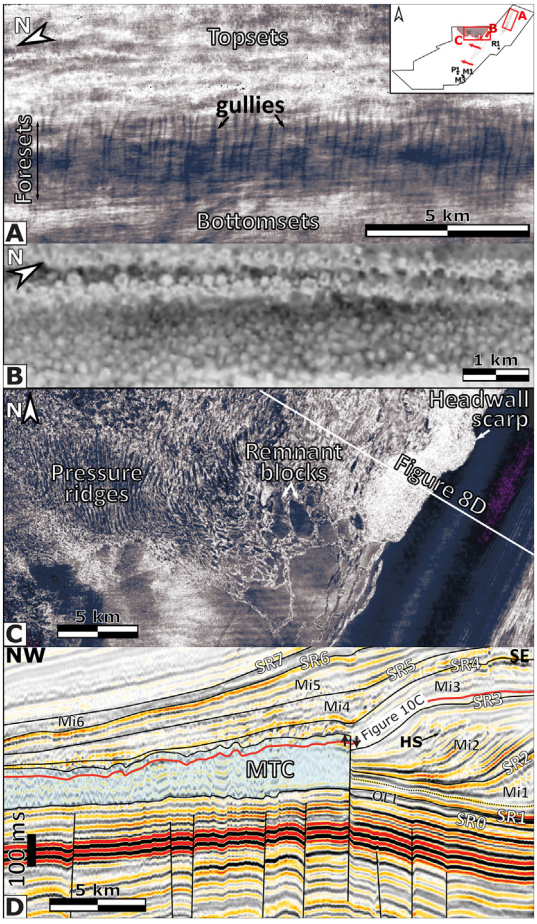

Fig. 10. Seismic geomorphologies observed along Oligocene to early Miocene clinoforms (i.e., distally steepened ramp; sequences OL1-Mi3). A. Horizon-slice view with an envelope attribute showing linear, closely spaced headless gullies located on foresets of sequence OL1. B. Horizon slice with an envelope attribute presenting the time-transgressive Honeycomb Structure (HS) of inferred diagenetic origin. C. Horizon slice with an envelope attribute displaying a Mass Transport Complex (MTC) cutting through lower part of sequence Mi3 and older strata. D. Dip-oriented section of carbonate margin highlighting the relationship between MTC, HS and seismic sequences. Data courtesy of PGS.

outcrops. They are most easily interpreted in quarry walls (Fig. 13A–B). Several karstified levels were observed (Fig. 13C), as well as diverse assemblages of corals, including coral pillarstone (Fig. 13D).

5.4. Serravallian

Seismic sequence Mi6 (Table 2) displays sub-parallel to chaotic seismic reflectors draping Mi5. It is almost exclusively restricted to the more proximal part of the northern depocenter and Novara Arch area, where it locally reaches a thickness of 200 ms. It is very poorly developed in the Southern depocenter (Fig. 7). The only landform observable is a prominent curvi-linear ridge, which is present in the upper part of the sequence. This ridge, first described by Riera et al. (*in press*) is composed of stacked curvi-linear features with lobe morphologies, that mimic the morphology of the modern Ashburton delta coastline, and whose geometry is variating upward. Deeper deposits are mainly represented by thin sub-horizontal strata. Side-wall cores and cuttings from well Ramillies-1 indicate that the ridge is dominantly composed of quartz grains (Fig. 15I), and that it is overlying a level with quartz-rich coralline algae wackestone. There are no samples from the distal part of the sequence.

The lower part of this seismic sequence appears to be time-equivalent to outcrops of quartz-rich limestones (Fig. 15A–G). These outcrops, which are widespread in the northern part of the Water Corporation Land (Fig. 4) are dated between ~13.34 Ma and ~12.5 Ma by Riera et al. (2019b). These limestones differ from other Miocene limestones from Cape Range area as they contain common to abundant medium to coarse sub-angular to very well rounded quartz grains, which are visible with the naked eye (Fig. 15D–E). They also contain common coralline algal boundstones (Fig. 15B) and very rare metre-scale globose corals (Fig. 15A) and are interbedded with cross-bedded coarse quartz sandstones (Fig. 15C). Observations using an optical microscope reveal that the limestones are composed of peloidal grainstone to wackestone with common peloids, common miliolids, absent to common *Sorites* sp., rare dasycladal green algae, rare acervulinids, very rare to common planktic foraminifera and common to abundant quartz grains (Fig. 15F–G). However, the facies are highly variable, with for example *Sorites* sp. only present in the intervals with rare quartz grains, and planktic foraminifera most common in finer intervals. When present, the matrix is composed of micrite. The coralline algal boundstones are mainly composed of encrusting algae which have occasionally incorporated quartz grains in their internal structure (Fig. 15F).

The upper part of sequence Mi6, including the curvi-linear ridge, may be time-equivalent to the quartz sandstones of inferred Miocene age designated as Pilgramunna Formation present in the western part of the Cape Range anticline (Condon et al., 1955; Crespin, 1955). These sandstones are described as beach and soil deposits (Hocking et al., 1987) or siliciclastic deposits carried by longshore currents (Chaproniere, 1975). However, the age of these sandstones is poorly constrained, as they are only dated based on the observation of middle Miocene grains possibly reworked from the Trealla Limestone, such as broken *Lepidocyclina* sp. (Crespin, 1955) or *Lepidocyclina* (*N.*) *howchini-Marginopora vertabralis* (Chaproniere, 1975).

5.5. Post-Serravallian siliciclastics

The strata directly above seismic reflector SR7 (Table 2) are composed of stacked channel complexes, particularly dense in the Novara Arch area, where they seem to follow a ~10 km wide sediment fairway feeding a ~4 km wide and ~7 km long terminal fan complex (Fig. 17). Non-stacked channels are also present in the Northern depocenter, where they are up to 2 km wide, and have a low sinuosity. Study of well cuttings indicates that the proximal part of the sequence is dominantly composed of very fine to medium sub-rounded quartz grains in a micritic to clayey matrix (Fig. 18C–F). Debris of echinoderms and very rare stained *Amphistegina* sp. are locally present. These strata may be equivalent to the quartz sandstone of inferred Pliocene age designated as Vlaming Sandstone that is present in the western part of the Cape Range anticline (Condon et al., 1955; Crespin, 1955). These quartz sandstones comprise rounded quartz grains and locally infill karstified levels in the underlying limestone strata (Fig. 18A–B).

6. Discussion: margin evolution and palaeoenvironmental implications

Four depositional stages have arisen from the interpretation of seismic and outcrop data: (1) late Oligocene to early Miocene linear to sigmoidal carbonate clinoforms composed of foraminiferal wacke-packstone and micropackstone (sequences OL1-Mi3; Fig. 19A–D); (2) late Burdigalian-early Langhian carbonate drape associated with extensive dolomitization (sequence Mi4; Fig. 19E); (3) upper Langhian-lower Serravallian carbonate lagoon-barrier system, and associated slope channels (sequence Mi5; Fig. 19F); and (4) Serravallian siliciclastic seismic drape (sequence Mi6; Fig. 19G). Those depositional stages are separated by truncation surfaces, and illustrate the evolution of a carbonate-dominated margin across the Miocene.

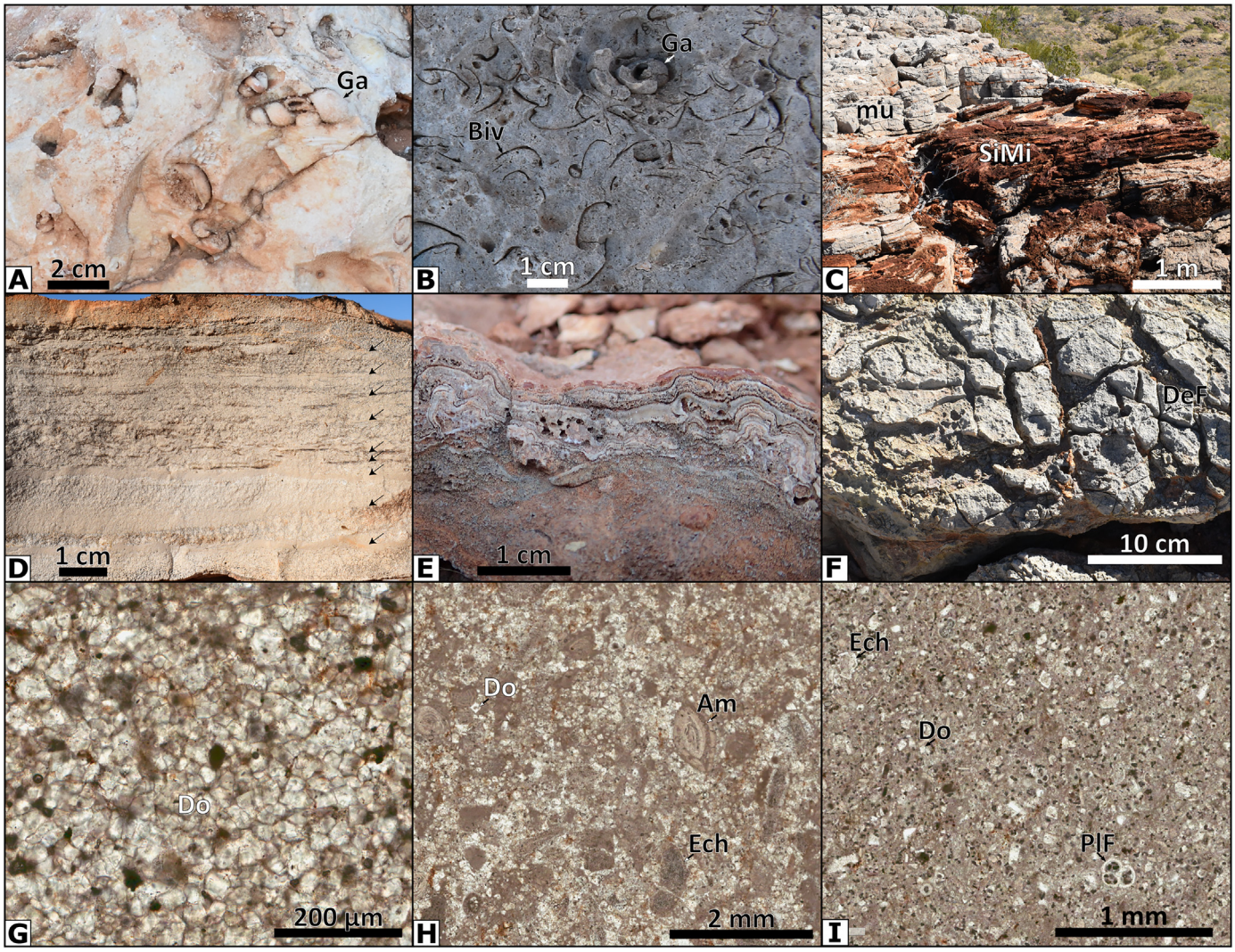

Fig. 11. Photographs and microphotographs of outcrops (A–F) and offshore facies (G–I; sequences Mi4) accumulated during the Miocene Climatic Optimum. A–F. Field photographs of outcrops interpreted as a fossilised sabkha, entrance of Shothole Canyon. A. Mudstone with gastropods (Ga). B. Coquina rudstone with abundant bivalves (Biv) and rare gastropods. C. Silicified finely laminated deposits interpreted as microbial laminites (SiMi) overlain by mudstone with fossil desiccation cracks (mu). D. Close-up view of banded deposit interpreted as fossil microbial laminites, note alternation of beige and white layers (indicated by black arrows). E. Domal structures of either microbial or diagenetic origin. F. Mudstone with polygonal cracks interpreted as fossil desiccation cracks (De). G. Microcrystalline dolomite from topset of sequence Mi4 (Macedon-3 429.5 mKB); H. Dolomitized foraminiferal wackestone with *Amphistegina* sp. (Am) and echinoderm debris from topset of sequence Mi4 (Ramillies-1 988 mKB). I. Micropackstone with echinoderm debris, planktic foraminifera and dolomite rhombs from uppermost part of bottomset of sequence Mi4 (Pyrenees-1 637 mKB).

6.1. Late Oligocene-early Miocene prograding clinoforms

The late Oligocene to early Miocene clinoforms (OL1, Mi1, Mi2, Mi3; Fig. 19A–D) form a thick sequence prograding on Palaeogene and Eocene strata. Interestingly, there is no sharp break at the Oligocene-Miocene transition. Late Oligocene clinoforms are linear, while clinoforms become sigmoidal during the Miocene, with a higher aggradation upward.

Facies analysis of the offshore part of the Mi1, Mi2 and Mi3 seismic sequences indicates that the clinoforms are mainly composed of marly micropakstone (Fig. 9E–F), with locally debris of flattened larger foraminifera (i.e., *Cycloclypeus* sp., *Lepidocyclina* (*Nephrolepidina*) sp. and *Operculina* sp.) in their lower topsets, hence indicating an accumulation of the lower topsets towards the base of the oligophotic zone or deeper. As no karst nor subaerial unconformities were observed within these sequences from field or seismic data, it can be inferred that the ramp observed in seismic data was deeply submerged, with the shelf break (i.e., clinoform rollovers) never emerged. This is consistent with previous observations by Cathro et al. (2003) and Moss et al. (2004) in the Dampier sub-basin. An accumulation in relatively deep waters is further supported by the absence of observation of coastal geomorphologies. As there is no evidence of submarine channels, with the exception of the headless gullies on the clinoform foresets of OL1 (Fig. 10A), it is proposed that sediments were transported along the clinoforms by currents and wave resuspension, as proposed for the clinoforms of the Dampier sub-basin (Cathro et al., 2003). The presence of dolomite rhombs, gypsum rosettes and seismic Honeycomb Structure might indicate clinoform compaction and diagenetic overprints during burial (Riera et al., 2019a).

Outcrop analysis indicates that the shallower part of the clinoforms (upper topsets) are composed of foraminiferal packstone (Fig. 9A–C). The shallowing-upward trend observed along the outcrops match well with the interpretation of a prograding system. As the uppermost part of all outcrops is eroded, the shallowest part of the ramp is not preserved in Cape Range anticline. It appears to be represented by the lagoonal limestone colonised by seagrass meadows outcropping in the Giralia Range anticline (Haig et al., 2020; Fig. 4). This further supports the view of a carbonate ramp,

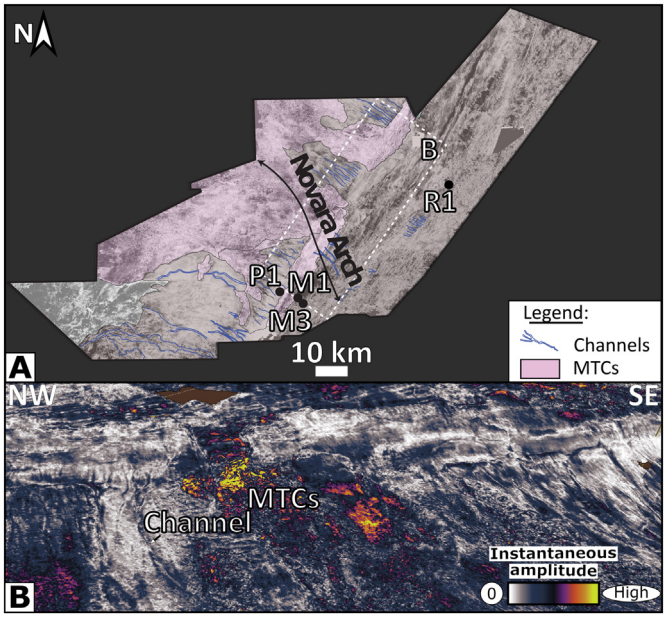

Fig. 12. A. Interpreted horizon slice with an envelope attribute of base sequence Mi4, indicating location of Mass Transport Complexes (MTCs) and slope channels. B. Three-dimensional view of the same horizon with an Instantaneous amplitude attribute highlighting seismic character of MTCs and channels. Data courtesy of PGS.

without any marked break along its depositional profile, dominantly composed of foraminiferal tests and micropackstone, with the facies partitioning controlled by water depth (Riera et al., 2022). A barrier could have been present in the Rough Range area, hence separating the marginal lagoonal from the open ocean ramp (Haig et al., 2020). As already pointed out by Riera et al. (2022), the presence of early Miocene larger benthic foraminifera with tropical affinities within the seismic sequences Mi1, Mi2 and Mi3 indicates a formation of those clinoforms in warm waters. These warm waters may either indicate the existence of a south-flowing Leeuwin current during the early Miocene (Feary and James, 1995; McGowran et al., 1997; O'Connell et al., 2012; Wyrwoll et al., 2009), or are a direct consequence of the overall warm climate during the early Miocene (Mudelsee et al., 2014). Formation of a major MTC during the accumulation of the sequence Mi3 (Fig. 10C), with its headwall scarp aligned with an underling fault, might indicate the onset of the Miocene structural inversions in the area.

6.2. Early-middle Miocene sabkha and MTDs

The sequence Mi4 has a different seismic character compared to the sequences OL1-Mi3, as it is not accumulated as a clinoform, but as a drape. In addition, it contains small channels in its distal part, and MTCs are often reworking its bottomsets. Its topsets are dolomitized. The only outcrop time-equivalent to the sequence Mi4 is present at the entrance of the Shothole Canyon (Figs. 4, 11). This outcrop is here interpreted as a fossilised sabkha deposit, in line with Collins et al. (2006), as it contains gastropod layers, coquina rudstone and fossilised microbial mats, which might indicate an accumulation in a hypersaline and highly stressed environment (Court et al., 2017; James and Jones, 2015). The presence of microbial mats is inferred from the observation of laminated deposits (Fig. 11D), possibly representing an alternation of clean sediment with sediment bounded by microbial mat (Jahnert and Collins, 2013; Riding, 2011; Vasconcelos et al., 2014). Microbial activity is further supported by the presence of domal structures with pustules (Fig. 11E) similar in shape and size to columnar non-branching stromatolites (Jahnert and Collins, 2013; Riding, 2011; Vasconcelos

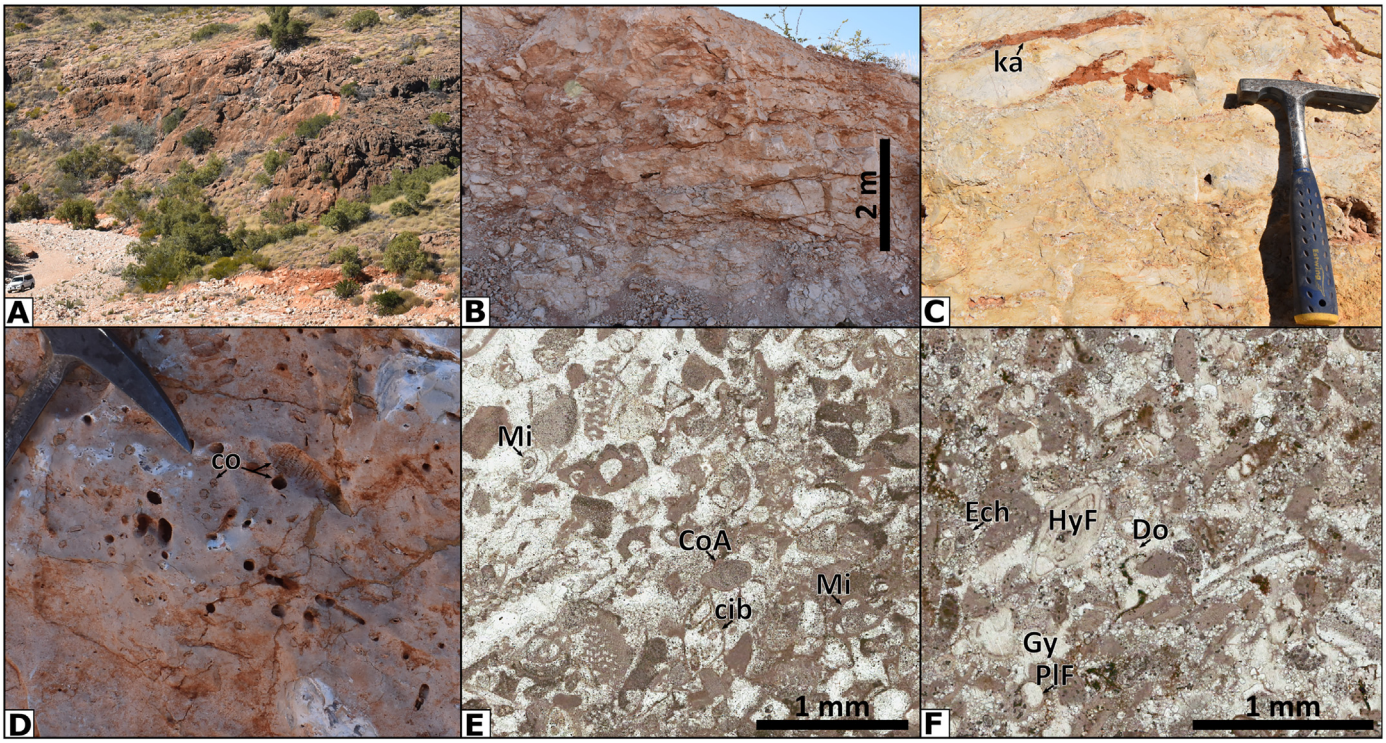

Fig. 13. Field photographs and microphotographs of the lagoonal facies present onshore (A–D) and of time-equivalent facies present offshore (E–F; sequences Mi5). A–B. Field photographs illustrating typical outcrops present in Mowbowrra Creek area, respectively in the vicinity of Exmouth Limestone Quarry and Exmouth Concrete Quarry. C. Well-cemented lagoonal limestone with karsts (ka), Exmouth Limestone Quarry. D. Branching coral float-pillarstone from the Exmouth Concrete Quarry, note that corals are exclusively recorded as moulds. E. Peloidal grainstone, with abundant small miliolid foraminifera (Mi), common small hyaline foraminifera (cib) and rare coralline algae (CoA) from the uppermost part of sequence Mi5 (Ramillies-1 810 mKB). F. Dolomitized and leached wacke-packstone with hyaline foraminifera (HyF), echinoderm debris (Ech), planktic foraminifera (PlF) and abundant dolomite rhombs (Do), note the presence of gypsum cements (Gy), the cutting is coming from the topset of the sequence Mi5 (Macedon-1 435 mKB).

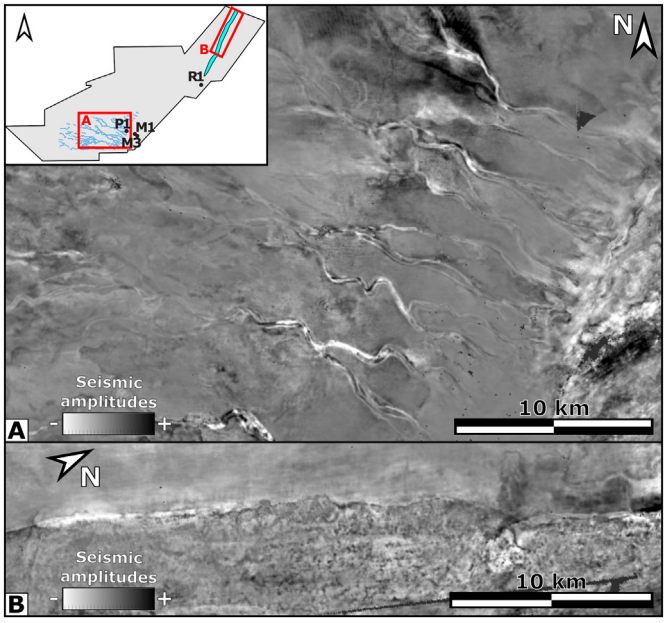

Fig. 14. Horizon slices with envelope attribute from the sequence Mi5. A. Slope system with sub-parallel sinuous channels. B. Seafloor ridge interpreted as a carbonate barrier. Data courtesy of PGS.

et al., 2014). Accumulation in a very shallow environment is also suggested by the presence of mudstone with polygonal cracks (Fig. 11F). The extensive dolomitization observed onshore and offshore could be related to the sabkha formation, as low-temperature dolomitization is well documented in modern sabkha environments (e.g., Bontognali et al., 2010; DiLoreto et al., 2019; Petrash et al., 2017). In addition, dolomite is reported in Miocene sabkha from the Roebuck Basin (northern part of the NWS, Petrick et al., 2019). It has also been proposed by previous studies that extensive dolomitization could be the result of hyper-saline brine reflux (Wallace et al., 2003). Sabhka formation might indicate a climate aridification concomitant to the MCO, and it can be correlated with a major decrease in relative sea level associated with karstification (partial platform emersion; Cathro et al., 2003; Collins et al., 2006). The abundance of MTCs within seismic sequence Mi4 (Fig. 12) could indicate more frequent slope failures and instability, possibly related to a sustained tectonic activity or important eustatic variations during the formation of this sequence.

6.3. Middle Miocene lagoon-barrier system

Sequence Mi5 also forms a seismic drape, with its upper part equally eroded. It stands out because of the presence of the seismic ridge (Fig. 14B), and of the well-developed slope channels (Fig. 14A). The seismic ridge is time-equivalent to lagoonal outcrops (Fig. 13A–D; Riera et al., 2021), and as such, the ridge is interpreted as a barrier. Facies observed within the offshore part of the ridge-lagoon system, with packstone and grainstone containing miliolids, large hyaline foraminifera and debris of coralline algae, have similarities with the lagoonal limestones outcropping in Cape Range anticline (Fig. 13). The ridge has striking morphological similarities to the modern Australian shoreline, and as such it is proposed it could either be: (1) a coralgal reefal

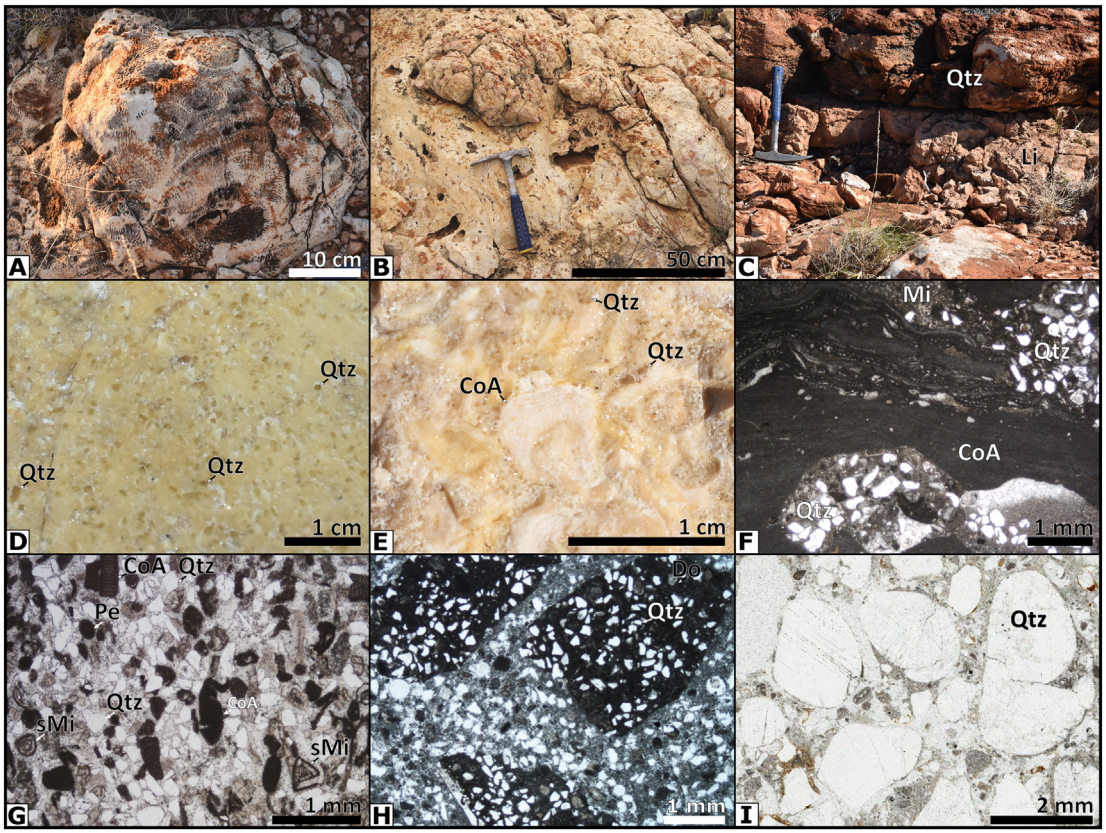

Fig. 15. Field photographs and thin-section images of quartz-rich Serravallian limestones from the northern part of Water Corporation Land (A–G) and microphotographs of the curvi-linear ridge at offshore well Ramillies-1 (H–I, sequence Mi6). A. Field photograph of a fossil dome-shaped hard coral colony. B. Field photograph of a massive coralline algae boundstone. C. Field photograph of a peloidal limestone containing common quartz grains (Li) overlaid by a quartz sandstone (Qtz). D. Close view photograph of a limestone with abundant medium angular quartz grains. E. Close view photograph of a quartz-rich coralline algae boundstone, note the abundance of quartz grains (Qtz) around the algae (CoA). F. Microphotograph of a coralline algae boundstone (CoA) with its internal porosity filled with quartz (Qtz) and micrite (Mi). G. Microphotograph of a quartz sandstone (Qtz) with peloids (Pe), coralline algae (CoA) and small miliolids (sMi). H. Very fine to fine sandstone (Ramillies-1 769 mKB). I. Coarse to very coarse sandstone (Ramillies-1 580 mKB).

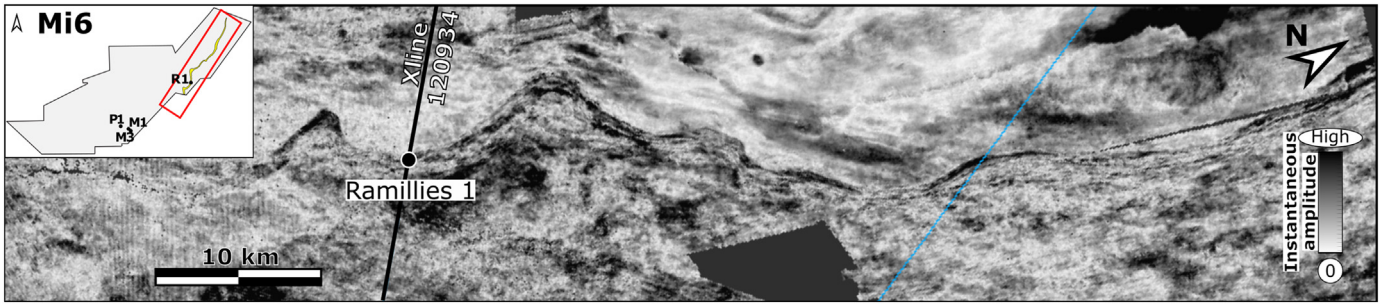

Fig. 16. Horizon slice with envelope attribute displaying the curvi-linear ridge from the sequence Mi6, interpreted as a siliciclastic palaeoshoreline. Data courtesy of PGS.

barrier developed on drowned coastal features (Belize Barrier Reef type, see Droxler and Jorry, 2013), or (2) a stack of beachrocks and aeolianites preserved through early cementation (drowned shoreline barrier type, see Salzmann et al., 2013 and Lebrec et al., 2022). The latter is supported by the linearity of the ridge, and by the absence of observation of reefal bioconstructions along outcrops. A formation of the ridge by mid-ramp mesophotic corals (type Yadana buildups, see Teillet et al., 2020) is not regarded as a likely hypothesis here, as corals are observed associated with organisms living in very shallow water such as *Flosculinella* sp., *Austrotrillina* sp. and green algae. In addition, corals are rare to absent in the deeper part of the lagoon (Riera et al., 2021). As the ridge is located in a mid-platform setting (Fig. 5), its presence might indicate a partial emersion of the shelf during the middle Miocene. Evidence for shelf exposure along the NWS during the middle Miocene, such as karsts, have already been reported, both from onshore outcrops (Matonti et al., 2021; Riera et al., 2021) and offshore seismic data (Cathro and Austin, 2001; Tagliaro et al., 2018). This emersion might be due to the expansion of the Antarctic ice sheets concomitant to the MMCT (Frigola et al., 2021). The nature of the facies forming the slope channels is unknown, as they are neither collected by offshore wells nor outcropping. However, the presence of those channels could be an indication of a high carbonate production within the lagoon. Finally, the absence of quartz grains in the cuttings suggests an absence of river activity, which supports a continental aridification during the middle Miocene (Groeneveld et al., 2017).

6.4. Serravallian siliciclastic influx

Sequence Mi6 also forms a drape, and also contains a ridge, in its upper part. However, analysis of well data indicates it is a siliciclastic sequence with coarse quartz grains being a major component (Fig. 5). The curvi-linear ridge present in the upper part of the sequence is interpreted as a stack of siliciclastic deltaic features, because of the presence of lobes and of the apparent mobility of the different stacked features forming the ridge. This interpretation is supported by the location of the ridge in front of the modern Ashburton River delta (Fig. 19G), hence suggesting that this siliciclastic ridge corresponds to the palaeodelta of the Ashburton River.

The local presence of corals and coralline algae time-equivalent to the lower-part of the sequence Mi6 (Fig. 15A–B) indicates that a coralgal

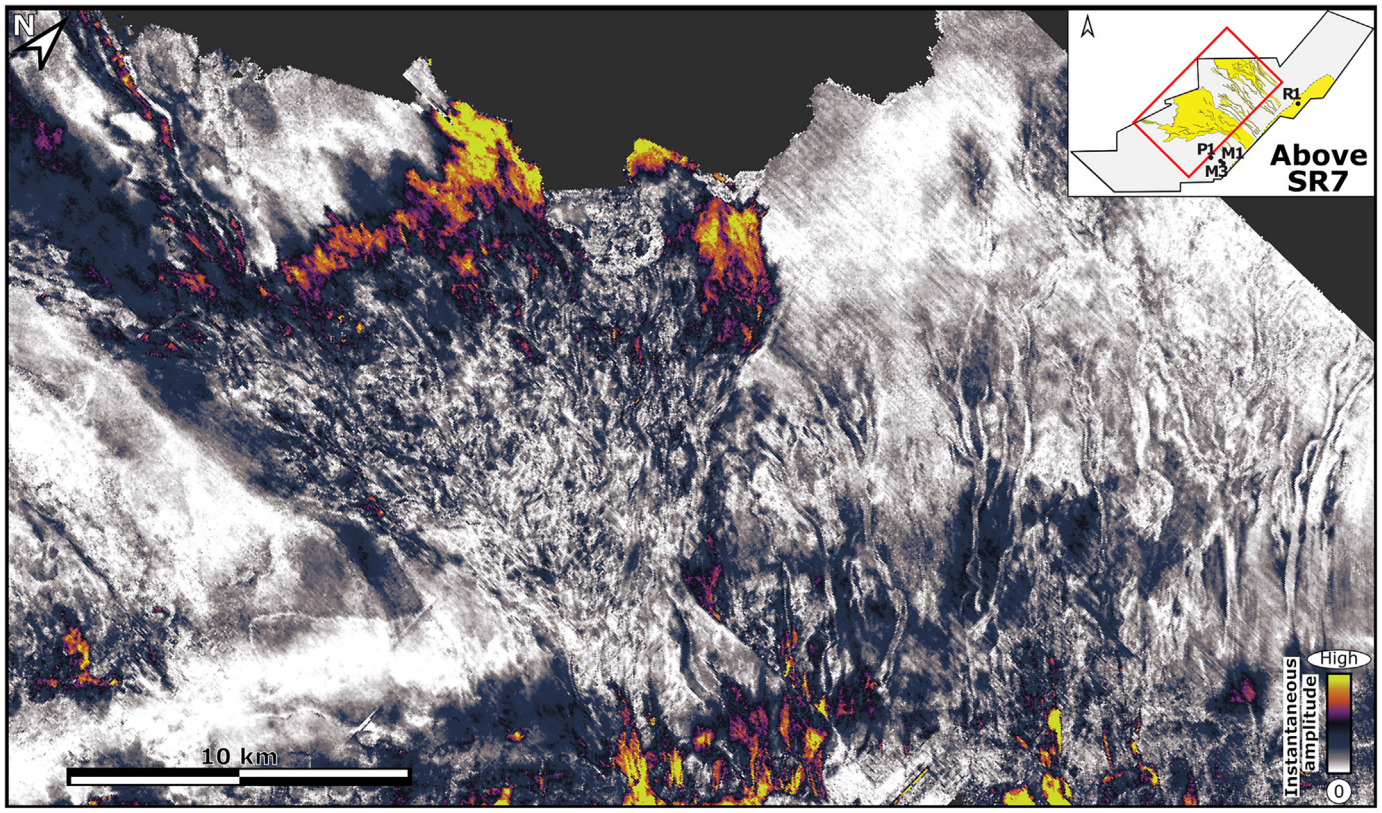

Fig. 17. Horizon slice with envelope attribute presenting the siliciclastic deposits overlying the seismic reflector SR7. Data courtesy of PGS.

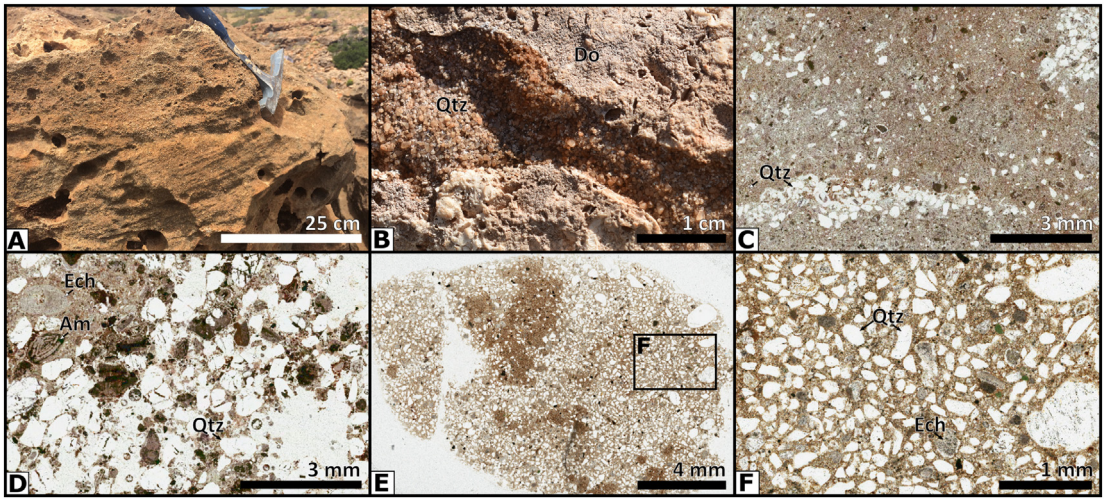

Fig. 18. Field photographs of sandstones (A–B) and thin-section images of offshore cuttings above reflector SR7 (C–F). A. Outcrop of coarse sandstone from the uppermost part of the Pilgonaman Gorge. B. Karst within dolomitized limestone (Do) filled by coarse quartz grains (Qtz) at the entrance of the Pilgonaman Gorge. C. Finely recrystallised limestone matrix containing undifferentiated carbonate grains (brown) and pockets filled with quartz grains (Macedon-3 359 mKB). D. Coarse quartz sandstone (Qtz) with scattered *Amphistegina* sp. (Am) and echinoderm debris (Ech) (Macedon-1 385 mKB). E–F. Fine quartz sandstone with echinoderm debris (Ech) (Ramillies-1 450 mKB).

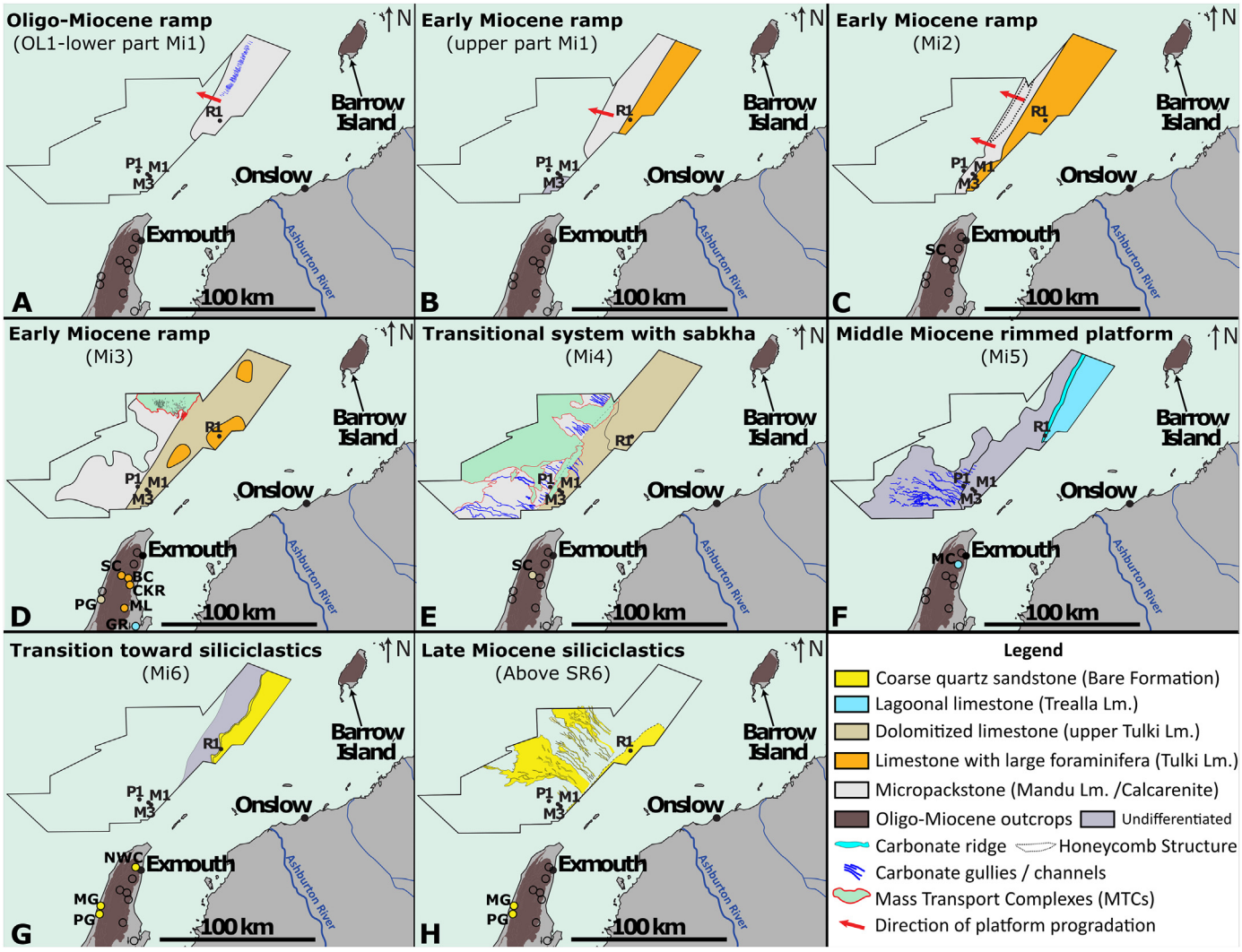

Fig. 19. Palaeomaps summarising evolution of Exmouth-Barrow margin through the Miocene, and showing the ramp (OL1-Mi3) to rimmed platform (Mi5) transition. Note the development of a sabkha depositional system concomitant to the MCO (Mi4), and the influx of siliciclastic sediments from the late middle Miocene onward (Mi6 and above SR6).

factory was locally active despite the influx of siliciclastic sediments. Those facies appear to be younger than the seismic ridge (Fig. 5), which might be time-equivalent to the coastal sandstones present in the western part of Cape Range anticline (Figs. 4, 18). The shift from a carbonate-dominated to a siliciclastic-dominated system could indicate a climate humidification, with a re-activation of fluvial runoff. Influx of quartz may have increased during the Serravallian and up to the late Miocene, as indicated by the presence of siliciclastic channels in strata overlying the sequence Mi6 (Figs. 17, 19H). Accumulation of these siliciclastic deposits appears relatively independent from seafloor palaeotopography, as they are largely accumulated on the Novara Arch, that was then forming a topographic high. This further suggests that the location of these siliciclastic sediments was not influenced by pre-existing topography, but by the location of their sources, inferred to be the palaeo-Ashburton River. The influx of quartz in the Exmouth-Barrow margin appears to be a regional event affecting most of the Northern Carnarvon Basin during the Serravallian, as it is also observed from outcrops in Cape Range anticline (Fig. 18). In addition, it is estimated the influx of quartz started after ~13/12.5 Ma across the Exmouth-Barrow margin (Figs. 16, 17), concomitant with the global cooling following the MMCT. This is broadly time-equivalent to the influx of quartz in the Dampier sub-basin area (Sanchez et al., 2012a, 2012b; Tagliaro et al., 2018). The cause of this regional event is still unclear, but it could well be correlated with the onset of an arid climatic interval (Tagliaro et al., 2018), or with the overall tilting of the NWS (Dicaprio et al., 2011; Czarnota et al., 2013).

7. Conclusion

This article presents the evolution of a carbonate-dominated margin during the Miocene. It is based on a unique combination of field, well and 3D seismic data, hence allowing the correlation of facies and seismic geomorphology at basin scale. Four main phases of deposition have been identified, which are concomitant to different Miocene climatic events: (1) the development of prograding carbonate clinoforms (ramp depositional profile) during the early Miocene global warming; (2) an episode of extensive dolomitization associated with sabkha formation onshore and MTCs development offshore, concomitant to the MCO; (3) the development of a barrier-lagoon system (rimmed platform) during the Miocene Climatic Transition; and (4) influx of siliciclastic sands during the Serravallian and late Miocene.

During the late Oligocene and early Miocene, clinoform prograding towards the north-west developed along the Exmouth-Barrow margin. Those clinoforms are dominantly composed of undifferentiated fine skeletal debris designated as micropackstone, in a clayey to micrite matrix, which is the only facies observed from the clinoform lower topsets to bottomsets. The foresets of those clinoforms form a ramp profile, which outcrops in Cape Range anticline. There, outcrops are shallowing-upward, with older outcrops composed of silty micropackstone and of foraminiferal wacke-packstone with *Cycloclypeus* sp., *Lepidocyclina* sp. and *Operculina* sp., and younger outcrops composed of wacke-grainstone with *Cycloclypeus* sp., *Lepidocyclina* sp., *Operculina* sp., *Sorites* sp., *Austrotrillina* sp., *Flosculinella* sp. and coralline algae. A marginal lagoon colonised by seagrass meadows, represented by miliolid-rich limestones outcropping in Giralia anticline, developed at the end of the early Miocene. As the facies containing light-dependant organisms such as larger benthic foraminifera are only present along the shallower part of the clinoform topsets, it is inferred that the lower topsets, foresets and bottomset of those clinoforms accumulated in the aphotic zone. Analysis of seismic geomorphologies present along those clinoforms reveals overall smooth clinoform fronts, with the most notable geomorphology, a Honeycomb Structure, inferred to be created by diagenetic reactions during clinoform burial. This fits well the view of clinoforms shaped by currents and sediment resuspension by waves. The presence of taxa with tropical affinities, such as *Cycloclypeus* sp. and *Flosculinella* sp., might indicate a warm environment during the Burdigalian.

The top of the younger clinoform is eroded, and it is overlayed by a partially dolomitized carbonate drape. The latter developed during the late Burdigalian-early Langhian, and is concomitant to the MCO. The exact depositional morphology of this sequence is unknown, because it is largely eroded in its proximal part, and is extensively reworked as Mass Transport Complexes in its distal part. A sabkha environment developed in Cape Range area during the MCO. It is represented by fossilised microbial mats, mudstone with polygonal cracks and coquina rudstone, and it might indicate a continental aridification during the MCO.

A carbonate lagoon-barrier system developed during the upper Langhian-lower Serravallian. It is associated with distal slope channels. The lagoon, that outcrops in Cape Range anticline, is composed of mudstone, porcelaneous foraminiferal pack-grainstone with corals and green algae, and peloidal wacke-grainstone. The barrier is interpreted as either a coralgal reefal barrier developed on drowned coastal features, or a stack of beachrocks and aeolianites preserved through early cementation. Its location, in a mid-platform setting, is interpreted as an indicator of at least one relative sea-level fall and palaeoshoreline development in the mid-platform, followed by at least one relative sea-level rise. Those sea-level variations were possibly driven by the expansion of the Antarctic ice sheets during the Miocene Climatic Transition. The latter is supported by the observation of karsts from onshore outcrops and offshore seismic data.

The Serravallian (late middle Miocene) is marked by a pulse of siliciclastic sediments. A coralgal factory has however persisted at the early stage of the siliciclastic pulse, as quartz-rich coralgal limestones, inferred to have accumulated between ~13.34 Ma and ~12.5 Ma, are documented in the northern part of Cape Range anticline. A seismic ridge post-dating those limestones subsequently developed. It is interpreted as a stack of siliciclastic deltaic coastlines, possibly representing the palaeo-Ashburton delta coastline. This ridge is interpreted as equivalent to the coastal siliciclastic sandstones present in the western part of the Cape Range anticline. The siliciclastic pulse appears to intensify after the Serravallian, with the development of stacked channel complexes imaged by 3D seismic data offshore, and the accumulation of quartz sandstones now outcropping in Cape Range anticline.

This study demonstrates that carbonate margins are records of the palaeoclimatology, palaeoceanography and palaeogeography of continental shelves. If they do not always offer continuous sedimentary record, the sedimentary facies that form them carry information on the environment in which they were deposited. In addition, the geomorphology of the sedimentary objects that they contain carry information on the depositional processes active during their formation. By documenting the evolution of the shelfal sedimentation along the Exmouth-Barrow margin (southern North West Shelf; area > 10,000 km^2) from the late Oligocene to late Miocene (time span >20 Ma), this study illustrates how combining 3D seismic, well and outcrop data can be used to identify regional and global palaeoenvironmental changes.

Data availability statement

3D reflection seismic data used for this research consist of public and PGS-owned seismic reflection data combined in a regional dataset by PGS (https://www.pgs.com/data-library/asia-pacific/nw-australia/northern-margin/north-carnarvon-basin/). SWC and well cuttings can be accessed through the Perth Core Library (https://www.dmp.wa.gov.au/Geological-Survey/Core-library-services-and-1391.aspx). Field samples are archived in the Edward de Courcy Clarke Earth Science Museum (University of Western Australia, Perth).

Declaration of competing interest

The authors declare that they have no known competing financial interests or personal relationships that influence the work reported in this paper.

Acknowledgments

The authors thank PGS for providing the Carnarvon MegaSurvey, the staff of the Perth Core Library for providing access to offshore well cuttings, the UWA:RM consortium for their financial support and Eliis for providing access to PalaeoScan™ software. The research was done as part of the first author's PhD thesis (Riera, 2020), and she acknowledges a postgraduate stipend and fees scholarship from the Centre for Energy Geoscience and the University of Western Australia respectively, and support from the Norwegian Geotechnical Institute (NGI) to write the paper. The authors are also very grateful to two anonymous reviewers, whose comments have been very helpful to improve the quality of the manuscript.

References

Allan, T.L., Trotter, J.A., Whitford, D.J., Korsch, M.J., 2000. Strontium isotope stratigraphy and the Oligocene-Miocene T-letter "stages" in Papua New Guinea. In: Buchanan, P. G., Grainge, A.M., Thornton, R.C.N. (Eds.), Papua New Guinea's Petroleum Industry in the 21st Century: Proceedings of the 4 th PNG Petroleum Convention, Port Moresby, 29th-31st May, 2000, pp. 155–168.

Anell, I., Wallace, M.W., 2020. A fine balance: accommodation dominated control of contemporaneous cool-carbonate shelf-edge clinoforms and tropical reef-margin trajectories, North Carnarvon Basin, Northwestern Australia. Sedimentology 67, 96–117. https://doi.org/10.1111/sed.12628.

Apthorpe, M., 1965. Correlation of Drill Holes, Mowbowra Creek Area, Cape Range, WA. Petrological Report No. M.6/65. The Broken Hill Proprietary Company Limited, Raw Materials & Exploration Department, Melbourne.

Apthorpe, M., 1988. Cainozoic depositional history of the North West Shelf. In: Purcell, P. G., Purcell, R.R. (Eds.), The North West Shelf, Australia. Proceedings of the Petroleum Exploration Society of Australia Symposium, Perth, WA, pp. 55–84.

Betzler, C., Eberli, G.P., 2019. Miocene start of modern carbonate platforms. Geology 47, 771–775. https://doi.org/10.1130/g45994.1.

Blow, W.H., 1969. Late Middle Eocene to Recent Planktonic Foraminiferal Biostratigraphy. Proc. First Int. Conf. Planktonic Microfossils, Geneva 19671 pp. 199–422.

Bontognali, T.R.R., Vasconcelos, C., Warthmann, R.J., Bernasconi, S.M., Dupraz, C., Strohmenger, C.J., Mckenzie, J.A., 2010. Dolomite formation within microbial mats in the coastal sabkha of Abu Dhabi (United Arab Emirates). Sedimentology 57, 824–844. https://doi.org/10.1111/j.1365-3091.2009.01121.x.

BouDagher-Fadel, M.K., 2018. Evolution and Geological Significance of Larger Benthic Foraminifera. Second edition. UCL Press, London, UK.

Burchette, T.P., Wright, V.P., 1992. Carbonate ramp depositional systems. Sedimentary Geology 79, 3–57. https://doi.org/10.1016/0037-0738(92)90003-A.

Campbell, I.R., Tait, A.M., Reiser, R.F., 1984. Barrow Island oilfield, revisited. Australian Petroleum Exploration Association Journal 24, 289–298.

Cathro, D.L., Austin, J.A., 2001. An early mid-Miocene, strike-parallel shelfal trough and possible karstification in the Northern Carnarvon Basin, northwest Australia. Marine Geology 178, 157–169. https://doi.org/10.1016/S0025-3227(01)00177-3.

Cathro, D.L., Karner, G.D., 2006. Cretaceous-Tertiary inversion history of the Dampier Subbasin, northwest Australia: insights from quantitative basin modelling. Marine and Petroleum Geology 23, 503–526. https://doi.org/10.1016/j.marpetgeo.2006.02.005.

Cathro, D.L., Austin, J.A.J., Moss, G.D., 2003. Progradation along a deeply submerged Oligocene-Miocene heterozoan carbonate shelf: how sensitive are clinoforms to sea level variations? American Association of Petroleum Geologists Bulletin 87, 1547–1574. https://doi.org/10.1306/05210300177.

Chaproniere, G., 1976. The Bullara Limestone, a new rock-stratigraphic unit from the Carnarvon Basin, Western Australia. BMR Journal of Australian Geology and Geophysics 1, 171–174.

Chaproniere, G.C.H., 1975. Palaeoecology of Oligo-Miocene larger Foraminiferida, Australia. Alcheringa: An Australasian Journal of Palaeontology 1, 37–58. https://doi.org/10.1080/03115517508619479.

Chaproniere, G.C.H., 1977. Studies on Foraminifera From Oligo-Miocene Sediments, North-West Western Australia. (PhD Thesis)the University of Western Australia.

Cohen, K.M., Finney, S.C., Gibbard, P.L., Fan, J.-X., 2018. The ICS International Chronostratigraphic Chart. The ICS International Chronostratigraphic Chart, pp. 199–204 https://doi.org/10.1111/j.1502-3931.1980.tb01026.x.

Collins, L.B., Read, J.F., Hogarth, J.W., Coffey, B.P., 2006. Facies, outcrop gamma ray and C-O isotopic signature of exposed Miocene subtropical continental shelf carbonates, North West Cape, Western Australia. Sedimentary Geology 185, 1–19. https://doi.org/10.1016/j.sedgeo.2005.10.005.

Condon, M.A., Johnstone, D., Perry, W.J., Crespin, I., 1953. The Cape Range structure, Western Australia. Australia BMR Bulletin, p. 21.

Condon, M.A., Johnstone, D., Perry, W.J., 1955. Cape Range structure Western Australia, part 1. Bureau of Mineral Ressources, Geology and Geophysics of the Commonwealth of Australia, Bulletin No. 21, 2nd edition, pp. 7–48.

Court, W.M., Paul, A., Lokier, S.W., 2017. The preservation potential of environmentally diagnostic sedimentary structures from a coastal sabkha. Marine Geology 386, 1–18. https://doi.org/10.1016/j.margeo.2017.02.003.

Crespin, I., 1955. The Cape Range structure, Western Australia - part 2. Bureau of Mineral Ressources, Geology and Geophysics of the Commonwealth of Australia, Bulletin No. 21, 2nd edition, pp. 49–81.

Crossman, S., Li, O., 2015. Surface Hydrology Lines (National). Geoscience Australia, Canberra. http://pid.geoscience.gov.au/dataset/ga/83130.

Czarnota, K., Hoggard, M.J., White, N., Winterbourne, J., 2013. Spatial and temporal patterns of Cenozoic dynamic topography around Australia. Geochemistry, Geophysics, Geosystems 14, 634–658. https://doi.org/10.1029/2012GC004392.

Davies, R.J., Stewart, S.A., Cartwright, J.A., Lappin, M., Johnston, R., Fraser, S.I., Brown, A.R., 2004. 3D seismic technology: are we realising its full potential? Geological Society Memoirs 29, 1–10. https://doi.org/10.1144/GSL.MEM.2004.029.01.01.

DePaolo, D.J., Kyte, F.T., Marshall, B.D., O'Neil, J.R., Smit, J., 1983. Rb-Sr, Sm-Nd, K-Ca, O and H isotopic study of Cretaceous-Tertiary boundary sediments, Caravaca, Spain: evidence for an oceanic impact site. Earth and Planetary Science Letters 64, 356–373.

Dicaprio, L., Gurnis, M., Müller, R.D., Tan, E., 2011. Mantle dynamics of continentwide Cenozoic subsidence and tilting of Australia. Lithosphere 3 (5), 311–316.

DiLoreto, Z.A., Bontognali, T.R.R., Al Disi, Z.A., Al-Kuwari, H.A.S., Williford, K.H., Strohmenger, C.J., Sadooni, F., Palermo, C., Rivers, J.M., McKenzie, J.A., Tuite, M., Dittrich, M., 2019. Microbial community composition and dolomite formation in the hypersaline microbial mats of the Khor Al-Adaid sabkhas, Qatar. Extremophiles 23, 201–218. https://doi.org/10.1007/s00792-018-01074-4.

Direen, N.G., Borissova, I., Stagg, H.M.J., Colwell, J.B., Symonds, P.A., 2007. Nature of the continent-ocean transition zone along the southern Australian continental margin: a comparison of the Naturaliste Plateau, SW Australia, and the central Great Australian Bight sectors. Geological Society - Special Publications 282, 239–263. https://doi.org/10.1144/SP282.12.

Driscoll, N.W., Karner, G.D., 1998. Lower crustal extension across the Northern Carnarvon basin, Australia: evidence for an eastward dipping detachment. Journal of Geophysical Research - Solid Earth 103, 4975–4991. https://doi.org/10.1029/97jb03295.

Droxler, A.W., Jorry, S.J., 2013. Deglacial origin of barrier reefs along low-latitude mixed siliciclastic and carbonate continental shelf edges. Annual Review of Marine Science 5 (1), 165–190. https://doi.org/10.1146/annurev-marine-121211-172234.

Dunham, R.J., 1962. Classification to the carbonate rocks according to depositional texture. In: Ham, W.E. (Ed.), Classification of Carbonate Rocks. AAPG, Tulsa, pp. 108–121.

Elders, C., Bernecker, T., 2019. Revising the structural elements map of the North West Shelf. Australian Exploration Geoscience Conference (AEGC), p. 2 (September 2019. Perth).

Feary, D.A., James, N.P., 1995. Cenozoic biogenic mounds and buried Miocene(?) barrier reef on a predominantly cool-water carbonate continental margin - Eucla Basin, western Great Australian Bight. Geology 23, 427–430. https://doi.org/10.1130/0091-7613(1995)023<0427:CBMABM>2.3.CO;2.

Flower, B.P., Kennett, J.P., 1994. The middle Miocene climatic transition: East Antarctic ice sheet development, deep ocean circulation and global carbon cycling. Palaeogeography Palaeoclimatology Palaeoecology 108, 537–555. https://doi.org/10.1016/0031-0182(94)90251-8.

Frigola, A., Prange, M., Schulz, M., 2018. Boundary conditions for the Middle Miocene Climate Transition (MMCT v1.0). Geoscientific Model Development 11, 1607–1626. https://doi.org/10.5194/gmd-11-1607-2018.

Frigola, A., Prange, M., Schulz, M., 2021. A dynamic ocean driven by changes in CO2 and Antarctic ice-sheet in the middle Miocene. Palaeogeography Palaeoclimatology Palaeoecology 579, 110591. https://doi.org/10.1016/j.palaeo.2021.110591.

Gradstein, F., Ogg, J., Smith, A., 2005. A Geologic Time Scale 2004. Cambridge University Press, Cambridge https://doi.org/10.1017/CBO9780511536045.

Groeneveld, J., Henderiks, J., Renema, W., McHugh, C.M., De Vleeschouwer, D., Christensen, B.A., Fulthorpe, C.S., Reuning, L., Gallagher, S.J., Bogus, K., Auer, G., Expedition 356 Scientists, 2017. Australian shelf sediments reveal shifts in Miocene Southern Hemisphere westerlies. Science Advances 3, e1602567. https://doi.org/10.1126/sciadv.1602567.

Haig, D.W., Smith, M.G., Riera, R., Parker, J.H., 2020. Widespread seagrass meadows during the Early Miocene (Burdigalian) in southwestern Australia paralleled modern seagrass distributions. Palaeogeography Palaeoclimatology Palaeoecology 555, 109846. https://doi.org/10.1016/j.palaeo.2020.109846.

Heath, R.S., Apthorpe, M.C., 1984. New formation names for the Late Cretaceous and Tertiary sequence of the southern North West Shelf. Records - Geological Survey of Western Australia 7, 1–35.

Herbert, T.D., Lawrence, K.T., Tzanova, A., Peterson, L.C., Caballero-Gill, R., Kelly, C.S., 2016. Late Miocene global cooling and the rise of modern ecosystems. Nature Geoscience 9, 843–847. https://doi.org/10.1038/ngeo2813.

Hickman, H., Strong, C.A., 2003. Dampier - Barrow Island, 1:250 000 Sheet Western Australia, in: 1:250 000 Sheet Western Australia. Second edition. Geological Survey of Western Australia, Perth, WA, p. 75.

Hillis, R.R., Sandiford, M., Reynolds, S.D., Quigley, M.C., 2008. Present-day Stresses, Seismicity and Neogene-to-Recent Tectonics of Australia's 'Passive' Margins: Intraplate Deformation Controlled by Plate Boundary Forces. Geol. Soc. London, Spec. Publ.306, pp. 71–90. https://doi.org/10.1144/SP306.3.

Hocking, R.M., Moors, H.T., Graaff, W.J., 1987. Geology of the Carnarvon Basin, Western Australia. Bulletin of the Geological Survey of Western Australia (Perth).

Holbourn, A., Kuhnt, W., Schulz, M., Erlenkeuser, H., 2005. Impacts of orbital forcing and atmospheric carbon dioxide on Miocene ice-sheet expansion. Nature 438, 483–487. https://doi.org/10.1038/nature04123.

Holbourn, A., Kuhnt, W., Kochhann, K.G.D., Andersen, N., Sebastian Meier, K.J., 2015. Global perturbation of the carbon cycle at the onset of the Miocene Climatic Optimum. Geology 43, 123–126. https://doi.org/10.1130/G36317.1.

Holbourn, A.E., Kuhnt, W., Clemens, S.C., Kochhann, K.G.D., Jöhnck, J., Lübbers, J., Andersen, N., 2018. Late Miocene climate cooling and intensification of southeast Asian winter monsoon. Nature Communications 9, 1584. https://doi.org/10.1038/s41467-018-03950-1.

I'Anson, A., Elders, C., McHarg, S., 2019. Marginal fault systems of the Northern Carnarvon Basin: evidence for multiple Palaeozoic extension events, North-West Shelf, Australia.

Marine and Petroleum Geology 101, 211–229. https://doi.org/10.1016/j.marpetgeo.2018.11.040.
Jahnert, R.J., Collins, L.B., 2013. Controls on microbial activity and tidal flat evolution in Shark Bay, Western Australia. Sedimentology 60, 1071–1099. https://doi.org/10.1111/sed.12023.
James, N.P., Jones, B., 2015. Origin of Carbonate Sedimentary Rocks. Wiley.
John, C.M., Karner, G.D., Mutti, M., 2004. δ18O and Marion Plateau backstripping: Combining two approaches to constrain late middle Miocene eustatic amplitude. Geology 32 (9), 829–832. https://doi.org/10.1130/G20580.1.
Keep, M., Haig, D.W., 2010. Tectonophysics deformation and exhumation in Timor: distinct stages of a young orogeny. Tectonophysics 483, 93–111. https://doi.org/10.1016/j.tecto.2009.11.018.
Keep, M., Harrowfield, M., Crowe, W., 2007. The Neogene tectonic history of the North West Shelf, Australia. Exploration Geophysics 38, 151–174. https://doi.org/10.1071/EG07022.
Lebrec, U., Riera, R., Paumard, V., 2022. Morphology and distribution of submerged palaeoshorelines: Insights from the North West Shelf ofAustralia. Earth-Science Reviews 224, 103864. https://doi.org/10.1016/j.earscirev.2021.103864.
Leutert, T.J., Auderset, A., Martínez-García, A., Modestou, S., Meckler, A.N., 2020. Coupled Southern Ocean cooling and Antarctic ice sheet expansion during the middle Miocene. Nature Geoscience 13, 634–639. https://doi.org/10.1038/s41561-020-0623-0.
Liebrand, D., Beddow, H.M., Lourens, L.J., Pälike, H., Raffi, I., Bohaty, S.M., Hilgen, F.J., Saes, M.J.M., Wilson, P.A., Van Dijk, A.E., Hodell, D.A., Kroon, D., Huck, C.E., Batenburg, S.J., 2016. Cyclostratigraphy and eccentricity tuning of the early Oligocene through early Miocene (30.1–17.1 Ma): Cibicides mundulus stable oxygen and carbon isotope records from Walvis Ridge Site 1264. Earth and Planetary Science Letters 450, 392–405. https://doi.org/10.1016/j.epsl.2016.06.007.
Longley, I.M., Buessenschuett, C., Clydsdale, L., Cubitt, C.J., Davis, R.C., Johnson, M.K., Marshall, N.M., Murray, A.P., Somerville, R., Spry, T.B., 2002. The North West Shelf of Australia–A Woodside Perspective. Sediment. Basins West. Aust. 3 Proc. Pet. Explor. Soc. Aust. Symp., pp. 27–88 https://doi.org/10.1017/CBO9781107415324.004.
Malcolm, R.J., Pott, M.C., Delfos, E., 1991. A new tectono-stratigraphic synthesis of the North West Cape Area. The APEA Journal 31, 154–174.
Marshall, N.G., Lang, S.C., 2013. A New Sequence Stratigraphic Framework for the North West Shelf, Australia. Sediment. Basins West. Aust. IV Proc. Pet. Explor. Soc. Aust. Symp. Perth, Aust pp. 1–23.
Matonti, C., Bourget, J., Fournier, F., Håkansson, E., Pellerin, M., Hong, F., Reijmer, J., 2021. Distinct petroacoustic signature in heterozoan and photozoan carbonates resulting from combined depositional and diagenetic processes. Marine and Petroleum Geology 128, 104974. https://doi.org/10.1016/j.marpetgeo.2021.104974.
McArthur, J.M., Howarth, R.J., 2005. Strontium isotope stratigraphy. In: Gradstein, F.M., Ogg, J.G., Smith, A.G. (Eds.), A Geologic Time Scale 2004. Cambridge University Press, Cambridge, pp. 96–105.
McCaffrey, J.C., Wallace, M.W., Gallagher, S.J., 2020. A Cenozoic Great Barrier Reef on Australia's North West shelf. Global and Planetary Change 184, 103048. https://doi.org/10.1016/j.gloplacha.2019.103048.
McGowran, B., Li, Q., Cann, J., Padley, D., McKirdy, D.M., Shafik, S., 1997. Biogeographic impact of the Leeuwin Current in Southern Australia since the late middle Eocene. Palaeogeography Palaeoclimatology Palaeoecology 136, 19–40. https://doi.org/10.1016/S0031-0182(97)00073-4.
McNamara, K.J., Kendrick, G.W., 1994. Cenozoic Molluscs and Echinoids of Barrow Island, Western Australia. Records of the Western Australian Museum 51, 50.
Mitchum, R.M.J., Vail, P.R., Thompson, S.I., 1977a. In: Payton, C.E. (Ed.)Seismic Stratigraphy—Applications to Hydrocarbon Exploration26. AAPG Memoir, pp. 53–62. https://doi.org/10.1306/M26490C4.
Mitchum, R.M.J., Vail, P.R., Sangree, J.B., 1977b. Seismic Stratigraphy and Global Changes of SeaLevel, Part 6: Stratigraphic Interpretation of Seismic Reflection Patterns in Depositional Sequences. In: Payton, C.E. (Ed.), Seismic Stratigraphy—Applications to Hydrocarbon Exploration, AAPG Memoir. 26, pp. 117–134. https://doi.org/10.1306/M26490C8.
Moss, G.D., Cathro, D.L., Austin, J.A., 2004. Sequence biostratigraphy of prograding clinoforms, Northern Carnarvon Basin, Western Australia: a proxy for variations in oligocene to pliocene global sea level? Palaios 19, 206–226. https://doi.org/10.1669/0883-1351(2004)019<0206:SBOPCN>2.0.CO;2.
Mudelsee, M., Bickert, T., Lear, C.H., Lohmann, G., 2014. Cenozoic climate changes: a review based on time series analysis of marine benthic δ18O records. Reviews of Geophysics 52, 333–374. https://doi.org/10.1002/2013RG000440.Received.
Müller, R.D., Cannon, J., Qin, X., Watson, R.J., Gurnis, M., Williams, S., Pfaffelmoser, T., Seton, M., Russell, S.H.J., Zahirovic, S., 2018. GPlates: building a virtual earth through deep time. Geochemistry, Geophysics, Geosystems 19, 2243–2261. https://doi.org/10.1029/2018GC007584.
Mutti, M., Piller, W., Betzler, C., 2010. Miocene carbonatesystems: an introduction. In: Mutti, M., Piller, W., Betzler, C. (Eds.), Carbonate Systems During the Oligocene-Miocene Climatic Transition. Special PublicationNumber 42 of the International Association of Sedimentologists, pp. vii–xii.
O'Connell, L.G., James, N.P., Bone, Y., 2012. The Miocene Nullarbor Limestone, southern Australia; deposition on a vast subtropical epeiric platform. Sedimentary Geology 253–254, 1–16. https://doi.org/10.1016/j.sedgeo.2011.12.002.
Paumard, V., Bourget, J., Durot, B., Lacaze, S., Payenberg, T., George, A.D., Lang, S., 2019a. Full-volume 3D seismic interpretation methods: a new step towards high-resolution seismic stratigraphy. Interpretation 7, B33–B47. https://doi.org/10.1190/int-2018-0184.1.
Paumard, V., Bourget, J., Lang, S., Wilson, T., Riera, R., Gartrell, A., Vakarelov, B.K., Leary, M. O., George, A.D., 2019b. Imaging past depositional environments of the North West Shelf of Australia: lessons from 3D seismic data. In: Keep, M., Moss, S.J. (Eds.), The Sedimentary Basins of Western Australia V. Proceedings of the Petroleum Exploration Society of Western Australia Symposium. Perth, WA, p. 30.
Perrin, C., 2002. Tertiary: the emergence of modern reef ecosytems. In: Kiessling, W., Flügel, E., Golonka, J. (Eds.), Phanerozoic Reef Patterns. SEPM Special Publication72, pp. 587–621.
Petrash, Daniel A., Bialik, Or M., Bontognali, Tomaso R.R., Vasconcelos, Crisógono, Roberts, Jennifer A., McKenzie, Judith A., Konhauser, Kurt O., 2017. Microbially catalyzed dolomite formation: from near-surface to burial. Earth-Science Reviews 171, 558–582. https://doi.org/10.1016/j.earscirev.2017.06.015.
Petrick, B., Reuning, L., Martínez-García, A., 2019. Distribution of glycerol dialkyl glycerol tetraethers (GDGTs) in microbial mats from Holocene and Miocene sabkha sediments. Frontiers in Earth Science 7, 310. https://doi.org/10.3389/feart.2019.00310.
Pettijohn, F.J., Potter, P.E., Siever, R., 1972. Sand and Sandstone. Springer-Verlag, Berlin, Heidelberg, New York.
Pomar, L., 2001. Types of carbonate platforms: a genetic approach. Basin Research 13, 313–334. https://doi.org/10.1046/j.0950-091X.2001.00152.x.
Posamentier, H.W., Davies, R.J., Cartwright, J.A., Wood, L.J., 2007. Seismic geomorphology - an overview. Geological Society - Special Publications 277, 1–14. https://doi.org/10.1144/GSL.SP.2007.277.01.01.
Posamentier, H.W., Paumard, V., Lang, S.C., 2022. Principles of seismic stratigraphy and seismic geomorphology I: extracting geologic insights from seismic data. Earth-Science Reviews 228, 103963.
Powers, M.C., 1953. A new roundness scale for sedimentary particles. Journal of Sedimentary Petrology 23, 117–119.
Purcell, P.G., Purcell, R.R., 1988. The North West Shelf, Australia - An Introduction. North West Shelf, Aust. Based Proc. North West Shelf Symp. pp. 3–15.
Rankey, E.C., 2017. Seismic architecture and seismic geomorphology of heterozoan carbonates: Eocene-Oligocene, Browse Basin, Northwest Shelf, Australia. Marine and Petroleum Geology 82, 424–443. https://doi.org/10.1016/j.marpetgeo.2017.02.011.
Rexilius, J.P., Powell, S.L., 1994a. Micropalaeontological Analysis Macedon-1, Permit WA-155P, Carnarvon Basin.
Rexilius, J.P., Powell, S.L., 1994b. Micropalaeontological Analysis Pyrenees-1, Permit WA-155P, Carnarvon Basin.
Riding, R., 2011. The nature of stromatolites: 3,500 million years of history and a century of research. In: Reitner, J., Quéric, N.-V., Arp, G. (Eds.), Lecture Notes in Earth Sciences: Advances in Stromatolite Geobiology. Springer-Verlag, Berlin Heidelberg, pp. 29–74 https://doi.org/10.1007/978-3-642-10415-2.
Riera, R., 2020. Stratigraphic Evolution of Miocene Carbonate Platforms of the North West Shelf (Exmouth-Barrow Sub-Basins, Australia). PhD ThesisThe University of Western Australia https://doi.org/10.26182/5f2cbf672504d.
Riera, R., Bourget, J., Paumard, V., Wilson, M.E.J., Shragge, J., George, A.D., Borgomano, J., Wilson, T., 2019a. Discovery of a 400 km2 honeycomb structure mimicking a regional unconformity on three-dimensional seismic data. Geology 47, 1181–1184. https://doi.org/10.1130/g46484.1.
Riera, R., Haig, D.W., Bourget, J., 2019b. Stratigraphic revision of the Miocene Trealla Limestone (Cape Range, Western Australia): implications for Australasian foraminiferal biostratigraphy. Journal of Foraminiferal Research 49, 318–338. https://doi.org/10.2113/gsjfr.49.3.318.
Riera, R., Bourget, J., Håkansson, E., Paumard, V., Wilson, M.E.J., 2021. Middle Miocene tropical oligotrophic lagoon deposit sheds light on the origin of the Western Australian coral reef province. Palaeogeography Palaeoclimatology Palaeoecology 576, 110501. https://doi.org/10.1016/j.palaeo.2021.110501.
Riera, R., Bourget, J., Allan, T., Hakånsson, E., Wilson, M.E.J., 2022. Early Miocene carbonate ramp development in a warm ocean, North West Shelf, Australia. Sedimentology 69, 219–253. https://doi.org/10.1111/sed.12917.
Riera, R., Lebrec, U., Lang, S.C., Paumard, V., n.d.. Differentiating reefal ridgesfrom relict coastal ridges: Lessons from the geomorphologic study of buried Miocene buildups (North West Shelf, Australia) (Basin Research).
Romine, K.K., Durrant, J.M., 1996. Carnarvon Cretaceous-Tertiary Tie Report. Australian Geological Survey Organisation (AGSO).
Romine, K.K., Durrant, J.M., Cathro, D.L., Bernardel, G., 1997. Petroleum play element prediction for the Cretaceous-Tertiary basin phase, Northern Carnarvon Basin. APPEA Journal 37, 315–339.
Rosleff-Soerensen, B., Reuning, L., Back, S., Kukla, P., 2012. Seismic geomorphology and growth architecture of a Miocene barrier reef, Browse Basin, NW-Australia. Marine and Petroleum Geology 29, 233–254. https://doi.org/10.1016/j.marpetgeo.2010.11.001.
Rosleff-Soerensen, B., Reuning, L., Back, S., Kukla, P.A., 2016. The response of a basin-scale Miocene barrier reef system to long-term, strong subsidence on a passive continental margin, Barcoo Sub-basin, Australian North West Shelf. Basin Research 28, 103–123. https://doi.org/10.1111/bre.12100.
Ryan, D.A., Brooke, B.P., Collins, L.B., Kendrick, G.A., Baxter, K.J., Bickers, A.N., Siwabessy, P. J.W., Pattiaratchi, C.B., 2007. The influence of geomorphology and sedimentary processes on shallow-water benthic habitat distribution: Esperance Bay, Western Australia. Estuarine, Coastal and Shelf Science 72, 379–386. https://doi.org/10.1016/j.ecss.2006.10.008.
Ryan, G.J., Bernardel, G., Kennard, J.M., Jones, A.T., Logan, G.A., Rollet, N., 2009. A precursor extensive Miocene reef system to the Rowley Shoals reefs, WA: evidence for structural control of reef growth or natural hydrocarbon seepage. APPEA Journal 49, 337–363. https://doi.org/10.1071/AJ08021.
Salzmann, L., Green, A., Cooper, J.A.G., 2013. Submerged barrier shoreline sequences on a high energy, steep and narrow shelf. Marine Geology 346, 366–374. https://doi.org/10.1016/j.margeo.2013.10.003.
Sanchez, C.M., Fulthorpe, C.S., Steel, R.J., 2012a. Middle Miocene-Pliocene siliciclastic influx across a carbonate shelf and influence of deltaic sedimentation on shelf

construction, Northern Carnarvon Basin, Northwest Shelf of Australia. Basin Research 24, 664–682. https://doi.org/10.1111/j.1365-2117.2012.00546.x.

Sanchez, C.M., Fulthorpe, C.S., Steel, R.J., 2012b. Miocene shelf-edge deltas and their impact on deepwater slope progradation andmorphology, Northwest Shelf of Australia. Basin Research 24, 683–698. https://doi.org/10.1111/j.1365-2117.2012.00545.x.

Sangiorgi, F., Bijl, P.K., Passchier, S., Salzmann, U., Schouten, S., McKay, R., Cody, R.D., Pross, J., Van De Flierdt, T., Bohaty, S.M., Levy, R., Williams, T., Escutia, C., Brinkhuis, H., 2018. Southern Ocean warming and Wilkes Land ice sheet retreat during the mid-Miocene. Nature Communications 9, 1–11. https://doi.org/10.1038/s41467-017-02609-7.

Saqab, M.M., Bourget, J., Trotter, J., Keep, M., 2017. New constraints on the timing of flexural deformation along the northern Australian margin: implications for arc-continent collision and the development of the Timor Trough. Tectonophysics 696–697, 14–36.

Seton, M., Müller, R.D., Zahirovic, S., Gaina, C., Torsvik, T., Shephard, G., Talsma, A., Gurnis, M., Turner, M., Maus, S., Chandler, M., 2012. Global continental and ocean basin reconstructions since 200Ma. Earth-Science Reviews 113, 212–270. https://doi.org/10.1016/j.earscirev.2012.03.002.

Shevenell, A.E., Kennett, J.P., Lea, D.W., 2004. Middle Miocene Southern Ocean cooling and Antarctic cryosphere expansion. Science (80-.) 305, 1766–1770. https://doi.org/10.1126/science.1100061.

Steinthorsdottir, M., Jardine, P.E., Rember, W.C., 2021. Near-future pCO2 during the hot Miocene climatic optimum. Palaeogeography, Palaeoclimatology 36. https://doi.org/10.1029/2020PA003900.

Tagliaro, G., Fulthorpe, C.S., Gallagher, S.J., McHugh, C.M., Kominz, M., Lavier, L.L., 2018. Neogene siliciclastic deposition and climate variability on a carbonate margin: Australian Northwest Shelf. Marine Geology 403, 285–300. https://doi.org/10.1016/j.margeo.2018.06.007.

Teillet, T., Fournier, F., Montaggioni, L.F., BouDagher-Fader, M., Borgomano, J., Braga, J.C., Villeneuve, Q., Hong, F., 2020. Development patterns of an oligo-mesophotic isolated carbonate buildup (Upper Burman Limestone), early Miocene, Yadana field, offshore Myanmar. Marine and Petroleum Geology 111, 440–460. https://doi.org/10.1016/j.marpetgeo.2019.08.039.

Thronberens, S., Back, S., Bourget, J., Allan, T., Ruening, L., 2022. 3-D seismic chronostratigraphy of reefs and drifts in the Browse Basin, NW Australia. GSA Bulletin 134 (11–12), 3155–3175. https://doi.org/10.1130/B36286.1.

Tindale, K., Newell, N., Keall, J., Smith, N., 1998. Structural evolution and charge history of the Exmouth Sub-basin, Northern Carnarvon Bain, Western Australia. In: Purcell, P.G., Purcell, R.R. (Eds.), The Sedimentary Basins of Western Australia 2. Proceedings of Petroleum Exploration Society of Australia Symposium. Perth, pp. 447–472.

van Buchem, F.S.P., Allan, T.L., Laursen, G.V., Lotfpour, M., Moallemi, A., Monibi, S., Motiei, H., Pickard, N.A.H., Tahmasbi, A.R., Vedrenne, V., Vincent, B., 2010. Regional stratigraphic architecture and reservoir types of the Oligo-Miocene deposits in the Dezful Embayment (Asmari and Pabdeh Formations) SW Iran. Geological Society - Special Publications 329, 219–263.

van de Graaff, W.J.E., Denman, P.D., Hocking, R.M., 1976. Emerged Pleistocene marine terraces on Cape Range, Western Australia. Geological Survey of Western Australia, Annual Report for 1975, pp. 62–70.

van de Graaff, W.J.E., Denman, P.D., Hocking, R.M., Baxter, J.L., 1980. Yanrey-Ningaloo, Western Australia, 1:250,000 Geological Series - Explanatory Notes. Geological Survey of Western Australia.

van de Graaff, W.J.E., Denman, P.D., Hooking, R.M., 1982. Onslow, Western Australia, 1:250,000 Geological Series - Explanatory Notes. Geological Survey of Western Australia.

Vasconcelos, C., Dittrich, M., McKenzie, J.A., 2014. Evidence of microbiocoenosis in the formation of laminae in modern stromatolites. Facies 60, 3–13. https://doi.org/10.1007/s10347-013-0371-3.

Veevers, J.J., Cotterill, D., 1978. Western margin of Australia: evolution of a rifted arch system. Bulletin Geological Society of America 89, 337–355. https://doi.org/10.1130/0016-7606(1978)89<337:WMOAEO>2.0.CO;2.

Wade, B.S., Pearson, P.N., Berggren, W.A., Pälike, H., 2011. Review and revision of Cenozoic tropical planktonic foraminiferal biostratigraphy and calibration to the geomagnetic polarity and astronomical time scale. Earth-Science Reviews 104, 111–142. https://doi.org/10.1016/j.earscirev.2010.09.003.

Wallace, M.W., Condilis, E., Powell, A., Redfearn, J., Auld, K., Wiltshire, M., Holdgate, G., Gallagher, S., 2003. Geological controls on sonic velocity in the CenozoicCarbonates of the Northern Carnarvon Basin, North West Shelf, Western Australia. The APPEA Journal 43 (1), 385–399. https://doi.org/10.1071/AJ02020.

Wentworth, C.K., 1922. A scale of grade and class terms for clastic sediments. Journal of Geology 30, 377–392.

Wyrwoll, K.-H., Greenstein, B.J., Kendrick, G.W., Chen, G.S., 2009. The palaeoceanography of the Leeuwin Current: implications for a future world. Journal of the Royal Society of Western Australia 92, 37–51.

Yeates, A.N., Bradshaw, M.T., Dickins, J.M., Brakel, A.T., Exon, N.F., Landgord, R.P., Mulholland, S.M., Totterdell, J.M., Yeung, M., 1987. The Westralian superbasin: an Australian link with Tethys. In: McKenzie, K.G. (Ed.), Proceedings of the International Symposium on Shallow Tethys 2. Wagga Wagga, pp. 199–213.

Young, H.C., Lemon, N.M., Hull, J.N.F., 2001. The Middle Cretaceous to Recent Sequence stratigraphic evolution of the Exmouth-Barrow Margin, Western Australia. APPEA Journal 41, 381–413.

Zachos, J., Pagani, M., Sloan, L., Thomas, E., Billups, K., 2001. Trends, global rhythms, aberrations in global climate 65Ma to present. Science (80-.) 292, 686–693. https://doi.org/10.1126/science.1059412.

Zachos, J.C., Dickens, G.R., Zeebe, R.E., 2008. An early Cenozoic perspective on greenhouse warming and carbon-cycle dynamics. Nature 451, 279–283. https://doi.org/10.1038/nature06588.